ESC European Society of Cardiology

Cardiovascular Research (2019) **115**, 1886–1906
doi:10.1093/cvr/cvz085

Long noncoding RNA *NEAT1* modulates immune cell functions and is suppressed in early onset myocardial infarction patients

Martina Gast[1†], Bernhard H. Rauch[2,3†], Arash Haghikia[1,4†], Shinichi Nakagawa[5,6], Jan Haas[7,8], Andrea Stroux[9], David Schmidt[1], Paul Schumann[1], Stefan Weiss[9], Lars Jensen[10], Adelheid Kratzer[1], Nicolle Kraenkel[1], Christian Müller[11,12], Daniela Börnigen[11,12], Tetsuro Hirose[13], Stefan Blankenberg[11,12], Felicitas Escher[4,14,15], Anja A. Kühl[16], Andreas W. Kuss[10], Benjamin Meder[7,8,17], Ulf Landmesser[1,4,18†], Tanja Zeller[11,12†], and Wolfgang Poller[1,4,19*†]

[1]Department of Cardiology, Charité-Universitätsmedizin Berlin, Campus Benjamin Franklin, Charite Centrum 11, Hindenburgdamm 30, 12200 Berlin, Germany; [2]Institute for Pharmacology, Universitätsmedizin Greifswald, Felix-Hausdorff-Strasse 3, 17487 Greifswald, Germany; [3]German Center for Cardiovascular Research (DZHK), Site Greifswald, Felix-Hausdorff-Strasse 3, 17487 Greifswald; [4]German Center for Cardiovascular Research (DZHK), Site Berlin, Hindenburgdamm 30, 12200 Berlin, Germany[5]RNA Biology Laboratory, RIKEN Advanced Research Institute, Wako, Saitama, 351-0198 Japan; [6]Faculty of Pharmaceutical Sciences, Hokkaido University, Kita-12 jo, Nishi 6-chome, Kita-ku, Sapporo 060-0812 Japan; [7]Department of Cardiology, Institute for Cardiomyopathies, University Hospital Heidelberg, Im Neuenheimer Feld 669, 69120 Heidelberg, Germany; [8]German Center for Cardiovascular Research (DZHK), Site Heidelberg, Im Neuenheimer Feld 669, 69120 Heidelberg, Germany; [9]Institute for Biometry and Clinical Epidemiology, Hindenburgdamm 30, 12200 Berlin, Germany; [10]Interfaculty Institute for Genetics and Functional Genome Research, University of Greifswald, Felix-Hausdorff-Strasse 8, 17475 Greifswald, Germany; [11]Clinic for General and Interventional Cardiology, University Heart Center Hamburg, Martinistrasse 52, 20246 Hamburg, Germany; [12]German Center for Cardiovascular Research (DZHK), Site Hamburg/Lübeck/Kiel, Martinistrasse 52, 20246 Hamburg, Germany; [13]Institute for Genetic Medicine, Hokkaido University, Sapporo 060-0815, Japan; [14]Institute of Cardiac Diagnostics and Therapy (IKDT), Hindenburgdamm 30, 12200 Berlin, Germany; [15]Department of Cardiology CVK, Hindenburgdamm 30, 12200 Berlin, Germany; [16]iPATH.Berlin—Core Unit Immunopathology, Charité—Universitätsmedizin Berlin, Berlin, Germany; [17]Department of Genetics, Genome Technology Center, Stanford University Medical School, Stanford, CA, USA; [18]Berlin Institute of Health (BIH), Anna-Louisa-Karsch-Strasse 2, 10178 Berlin, Germany; and [19]Berlin-Brandenburg Center for Regenerative Therapies (BCRT), Hindenburgdamm 30, 12200 Berlin, Germany;

Received 15 June 2018; revised 15 February 2019; editorial decision 23 March 2019; accepted 27 March 2019; online publish-ahead-of-print 29 March 2019

Time for primary review: 66 days

Aims Inflammation is a key driver of atherosclerosis and myocardial infarction (MI), and beyond proteins and microRNAs (miRs), long noncoding RNAs (lncRNAs) have been implicated in inflammation control. To obtain further information on the possible role of lncRNAs in the context of atherosclerosis, we obtained comprehensive transcriptome maps of circulating immune cells (peripheral blood mononuclear cells, PBMCs) of early onset MI patients. One lncRNA significantly suppressed in post-MI patients was further investigated in a murine knockout model.

Methods and results Individual RNA-sequencing (RNA-seq) was conducted on PBMCs from 28 post-MI patients with a history of MI at age ≤50 years and stable disease ≥3 months before study participation, and from 31 healthy individuals without manifest cardiovascular disease or family history of MI as controls. RNA-seq revealed deregulated protein-coding transcripts and lncRNAs in post-MI PBMCs, among which nuclear enriched abundant transcript (*NEAT1*) was the most highly expressed lncRNA, and the only one significantly suppressed in patients. Multivariate statistical analysis of validation cohorts of 106 post-MI patients and 85 controls indicated that the PBMC *NEAT1* levels were influenced ($P = 0.001$) by post-MI status independent of statin intake, left ventricular ejection fraction, low-density lipoprotein or high-density lipoprotein cholesterol, or age. We investigated *NEAT1*$^{-/-}$ mice as a model of *NEAT1* deficiency to evaluate if *NEAT1* depletion may directly and causally alter immune regulation. RNA-seq of *NEAT1*$^{-/-}$ splenocytes identified disturbed expression and regulation of chemokines/receptors, innate immunity genes, tumour necrosis factor (TNF) and caspases, and increased production of reactive oxygen species (ROS) under baseline conditions. *NEAT1*$^{-/-}$ spleen displayed anomalous T_{reg} and T_H cell differentiation. *NEAT1*$^{-/-}$ bone marrow-derived macrophages (BMDMs) displayed altered transcriptomes with disturbed chemokine/chemokine receptor expression, increased baseline phagocytosis ($P < 0.0001$), and attenuated proliferation ($P = 0.0013$). *NEAT1*$^{-/-}$ BMDMs

* Corresponding author. Tel: +49-30-450-513765; fax: +49-30-450-7513984, E-mail: wolfgang.poller@charite.de

† The first and last three authors contributed equally to the study.

responded to LPS with increased ($P < 0.0001$) ROS production and disturbed phagocytic activity ($P = 0.0318$). Monocyte-macrophage differentiation was deregulated in *NEAT1*$^{-/-}$ bone marrow and blood. *NEAT1*$^{-/-}$ mice displayed aortic wall CD68^{+} cell infiltration, and there was evidence of myocardial inflammation which could lead to severe and potentially life-threatening structural damage in some of these animals.

Conclusion The study indicates distinctive alterations of lncRNA expression in post-MI patient PBMCs. Regarding the monocyte-enriched *NEAT1* suppressed in post-MI patients, the data from *NEAT1*$^{-/-}$ mice identify *NEAT1* as a novel lncRNA-type immunoregulator affecting monocyte-macrophage functions and T cell differentiation. *NEAT1* is part of a molecular circuit also involving several chemokines and interleukins persistently deregulated post-MI. Individual profiling of this circuit may contribute to identify high-risk patients likely to benefit from immunomodulatory therapies. It also appears reasonable to look for new therapeutic targets within this circuit.

Keywords Cardiovascular innate immunity • Early myocardial infarction • Immunoregulatory genes • Long noncoding RNA • Pattern recognition receptors

1. Introduction

Myocardial infarction (MI) is a leading cause of mortality worldwide, but commonly a disease of middle-aged and elderly populations. MI in young adults is relatively rare and multiple evidence suggests a specific genetic/epigenetic background in these patients, beyond established risk factors. Inflammation is a key driver of atherosclerosis, and in addition to proteins and microRNAs (miRs), long noncoding RNAs (lncRNAs) are recently under investigation with regard to their role in the regulation of innate and acquired immunity. Knowledge of cellular lncRNA functions is very limited so far, however, and for few lncRNAs functional data are available.[1–3] A number of lncRNAs is known to be involved in the regulation of innate and acquired immunity (Supplementary material online, *Table S1*) but has not been investigated in the context of atherosclerosis so far. Myocardial transcriptome mapping of post-MI rodents and patients has identified novel heart-specific lncRNAs.[4] To our knowledge, however, no study has investigated post-MI patients' circulating immune cells by RNA-sequencing (RNA-seq) so far, although they constitute the crucial second side of the atherosclerotic process. Here, we report data suggesting that lncRNAs expressed in circulating immune cell may be critically involved in immune cell—vascular system interactions, too, thus modulating the complementary side of the process influenced by myocardially and vascularly expressed lncRNAs.[4]

In this study of peripheral blood mononuclear cells (PBMCs) from early onset MI patients we employed deep RNA-seq to obtain comprehensive immune cell transcriptomes and observed distinctive anomalies encompassing several lncRNAs. Among the deregulated lncRNAs, nuclear enriched abundant transcript (*NEAT1*) was the most highly expressed and the only one significantly suppressed in these patients. Using the *NEAT1*$^{-/-}$ animal model of Nakagawa *et al.*[5,6] we subsequently evaluated if isolated *NEAT1* deficiency *in vivo* directly and causally alters immune regulation. While the clinical data indicate altered lncRNA expression profiles in PBMCs from post-MI patients, the experimental studies of *NEAT1*$^{-/-}$ mice provide first direct evidence that *NEAT1* is a novel lncRNA-type immunoregulator *in vivo* affecting monocyte-macrophage function.

2. Patients and methods

For all animal and human studies approval was granted by the institutional ethics review board and the regulatory authorities. All animal procedures were performed conform to the guidelines from Directive 2010/63/EU of the European Parliament on animal protection. Investigation of human tissues was conform to the principles in the Declaration of Helsinki. Informed consent was given prior to inclusion of people in the study.

2.1 Young Myocardial Infarction study

The *Young Myocardial Infarction* (*MI Young*) *study* includes 200 individuals with a history of MI at age ≤50 years. Individuals were included according to the following criteria: (i) confirmed MI (positive ECG, increase in biomarkers of cardiac necrosis, clinical symptoms, and proof by coronary angiography), (ii) age at first MI ≤50 years, (iii) stable disease ≥3 months before study participation. As controls, 190 healthy individuals without manifest cardiovascular disease or family history of MI were employed. As test cohorts, 28 male patients and 31 male controls were drawn from this *MI Young Study*, first subjected to qPCR prescreening of the PBMC expression level of *NEAT1* and 12 selected other transcripts, and subsequently to RNA-seq analysis.

2.2 Gutenberg Young Myocardial Infarction Study

The *Gutenberg Young Myocardial Infarction Study* (GIS) includes 246 individuals with a history of MI at age ≤50 years. Individuals were invited to participate in *GIS* when same criteria as for *MI Young* were met. As controls, 499 individuals recruited at the same study centre without manifest cardiovascular disease were used. Written informed consent was obtained from all studies participants. The study protocols and sampling design were approved by the local ethics committee, and by local and federal data safety commissioners. As validation cohorts, 106 male patients and 85 male controls were drawn from this GIS study and subjected to qPCR validation screening of the PBMC expression levels of *NEAT1*.

2.3 Transcriptome mapping of human PBMCs by RNA-seq

From the *MI Young* and *GIS Study*, total RNA from PBMCs was isolated using Trizol/Chloroform extraction. Separation of PBMCs was conducted within 20 min after blood collection. In brief, 8 mL blood was collected using *CPT Cell Preparation Tube System* and centrifuged. After separation, cells were washed twice in ice-cold PBS containing 2 mM EDTA. Immediately after separation, washed cells were resuspended in *Trizol Reagent* and frozen at -20°C until isolation of RNA on the same day (maximal storage time 5 h). After thawing, 300 µL chloroform was

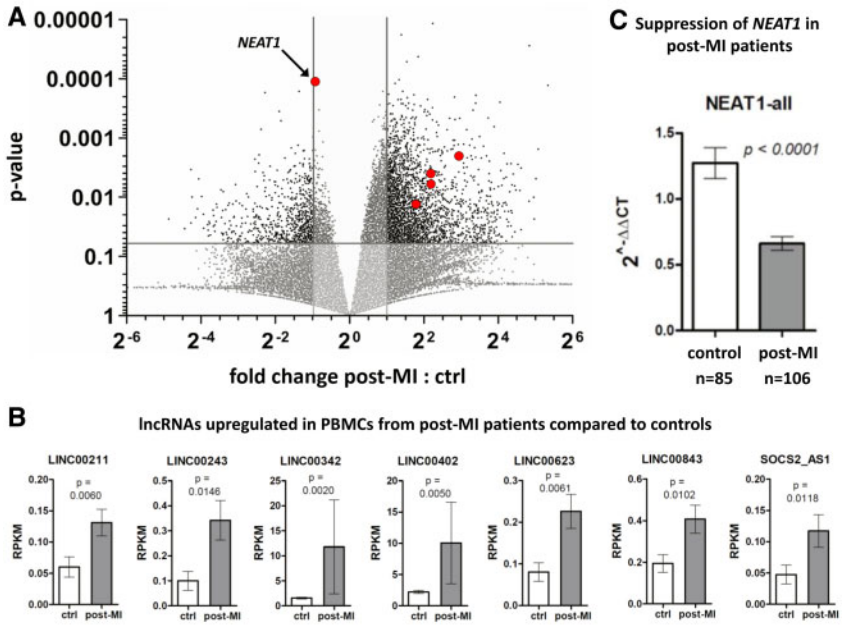

Figure 1 Anomalous lncRNA expression in post-MI patient PBMCs. (*A*) Volcano plot depicting transcript fold-change post-MI PBMCs ($n = 28$): control PBMCs ($n = 31$) vs. *P*-value. Only few lncRNAs were deregulated (red dots), whereas the far overwhelming number of all lncRNAs detected by RNA-seq were 'stably' expressed in post-MI vs. control PBMCs. For each transcript measured, the plot depicts the *P*-values obtained by Student's *t*-test comparing the test cohorts of 28 post-MI patients vs. 31 controls. (*B*) RNA-seq of test cohorts of 28 post-MI patients vs. 31 controls identified seven significantly up-regulated lncRNAs in post-MI PBMCs. So far nothing is known about the functions of these lncRNAs. To obtain the *P*-values for inter-group comparison of these test cohorts, Student's *t*-test was used. The mean values ± SEM are indicated. (*C*) Prescreening of test cohorts of 28 post-MI patients vs. 31 controls had shown that *NEAT1* was significantly down-regulated in patient PBMCs (Supplementary material online, *Table S2*). RNA-seq then detected that *NEAT1* was second highest among all lncRNAs expressed in PBMCs (*D*) and ≈10-fold more abundant than the next-highest expressed (NeST) with known immunoregulatory function. In validation cohorts of 106 post-MI patients vs. 85 controls, highly significant ($P < 0.0001$) *NEAT1* down-regulation was confirmed by qPCR. To obtain the *P*-value for inter-group comparison of these validation cohorts, Student's *t*-test was used. The mean values ± SEM are indicated. Multivariate statistical analysis of the validation cohorts showed that the *NEAT1* levels were determined by the post-MI status, independent of statin intake, LVEF, LDL or HDL cholesterol levels, age, diabetes, and smoking (*Table 1*). (*D*) lncRNA expression levels as determined by individual RNA-seq in 'healthy' human PBMCs, i.e. the PBMCs from the $n = 31$ test cohort control subjects. Indicated are mean values ± SEM. The grey triangle indicates the normal expression level of *NEAT1*, later found to be the only lncRNA significantly ($P < 0.0001$) down-regulated in post-MI vs. control PBMCs (*B*). Grey arrows indicate the normal PBMC expression levels of other lncRNAs with already known immunoregulatory functions. The absolute mean ± SEM RPKM expression levels of these lncRNAs in normal PBMCs are given in Supplementary material online, *Table S1*. *NEAT1* expression was ≈10-fold higher than the second-highest expressed immunoregulatory lncRNA (NeST). (*E*) All up-regulated lncRNAs as well as *NEAT1* (*D*) showed differential enrichment in immune cell subpopulations. RNA-seq analysis of their expression was conducted for five PBMC subpopulations (CD3+ T cells; CD4+ T helper cells; CD8+ cytotoxic T cells; CD4+ CD25+ regulatory T cells; CD19+ B cells; CD14+ monocytes). After FACS sorting of PBMCs from three healthy individuals, subtype RNA from all three individuals was pooled and RNA-seq done on these RNA pools. The resulting mean values are given for each transcript. (*F*) Strikingly differential expression was observed in these normal PBMC subpopulations for *NEAT1* and LINC00211, which were highly enriched in monocytes, distinct from the subtype-related expression of the others. In contrast, the level of the very high expressed *MALAT1* (not significantly deregulated in patients vs. controls) was rather homogeneous among these subpopulations (not shown).

added and phases separated by centrifugation. For RNA precipitation isopropanol was added and samples centrifuged at 12 000 *g* for 15 min. After washing with ethanol, the RNA pellet was dissolved in 40 µL RNase-free water, yield was checked measuring OD_{260} and OD_{260}/OD_{280} ratio, integrity of total RNA was evaluated by *Agilent Bioanalyzer 2100*. RNA samples were subsequently prepared with help of *TruSeq RNA sample prep Kit* (*Illumina*). Final libraries were clustered in batches of six samples per lane, to a concentration of 8 pmol. Sequencing was performed for 2 × 75 cycles (paired end). Generation of *fastq.gz* files was done with *CASAVA v.1.82*. RNA-Seq analysis was done using *CLC Genomics Workbench (v.6.5.1)*. Expression values are given as RPKM (reads per kilobase transcript per million reads). Data quality in the RNA-seq studies was high. In the mean, 5 GB and 6.5×10^7 reads were sequenced with 89 of bases ≥Q30 score.

Figures 1A–D and *2A–E* report the results of this 'individual RNA' RNA-seq conducted on 28 patients and 31 controls (means ± SEM depicted). In addition to these studies in humans, we conducted 'pooled RNA' RNA-seq analyses on splenocytes and bone marrow-derived macrophages (BMDMs) from mice. For these studies in *NEAT1*$^{-/-}$ vs. wild-type (WT) mice, splenocytes and BMDMs from four animals per group were isolated, treated with LPS vs. carrier, then total RNA was isolated (details below). RNA-seq was subsequently performed on RNA pooled

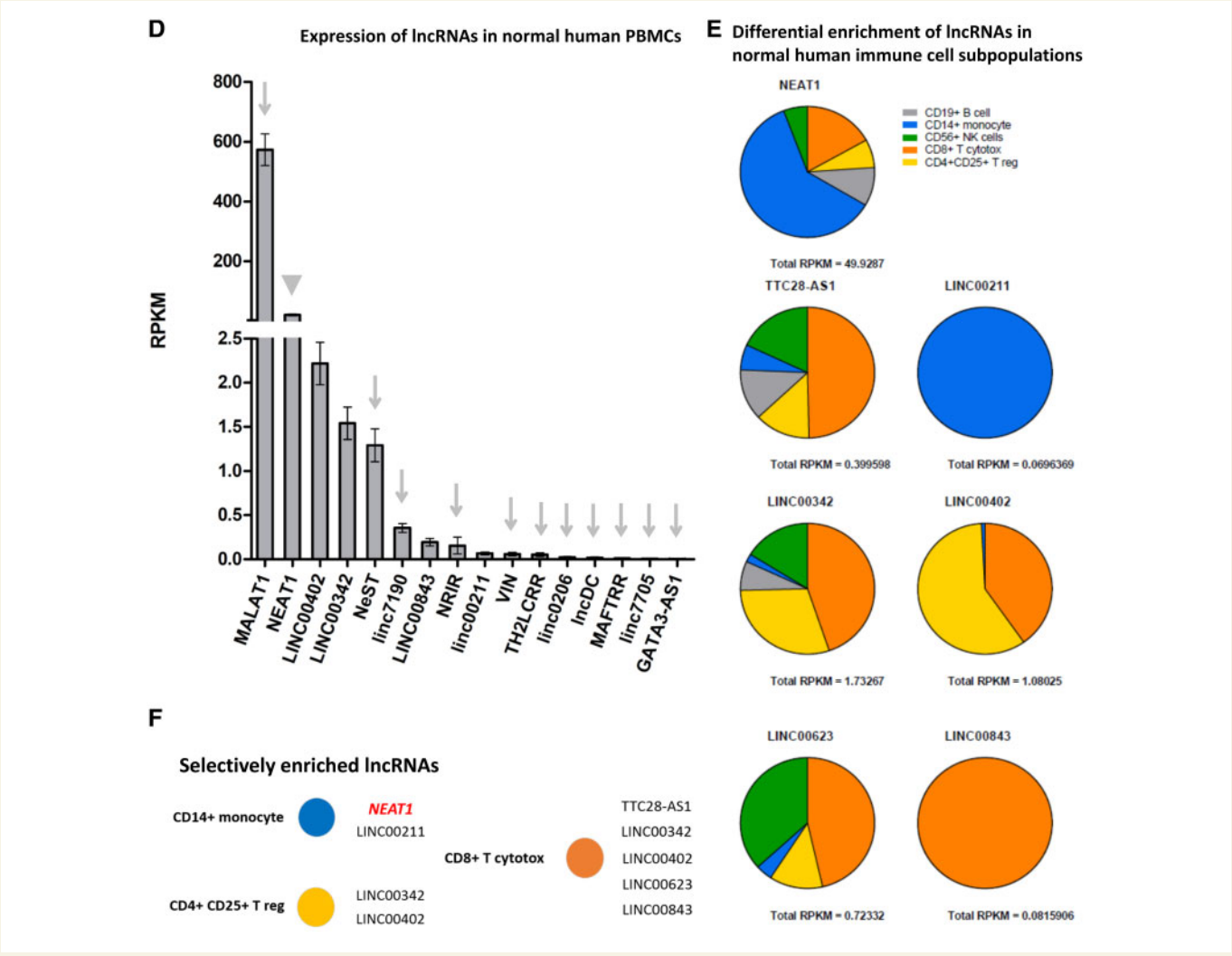

Figure 1 Continued.

from the respective cells. The results are reported in *Figures 1E, F* and *3E, G*, and *4I* which therefore display means only for the sequenced RNA pools.

2.4 Murine *NEAT1*$^{-/-}$ knockout model

For genotyping of the *NEAT1*$^{-/-}$ mice we used PCRs with primers and conditions as described.[5]

2.5 Cell culture studies

2.5.1 Murine bone marrow-derived macrophages

For the cell culture studies reported in *Figure 4D–I* (cell proliferation, phagocytic activity, intracellular reactive oxygen species (ROS) production, and gene expression by RNA-seq or qPCR) a large number of BMDM culture dished was prepared from a total of $n = 12$ WT and $n = 12$ *NEAT1*$^{-/-}$ mice. As many dishes as possible were seeded from each animal, dependent on the number of viable cells recovered from their femoral cavities.

BMDMs were derived from non-adherent macrophage precursors as follows. Maintenance, differentiation and growth of these precursors require medium containing macrophage colony-stimulating factor (M-CSF). Both femura were extracted from the mice and the ends were cut-off. A syringe with medium (DMEM containing high glucose, pyruvate, 10% FCS and 1% P/S) and a 25-G needle was used to flush the bone marrow cells from the cavity and gently resuspend them. Cells were collected at 350 × g for 8 min and washed once with medium. Cell pellet was resuspended in medium with 10 ng/mL recombinant M-CSF. Viable cells were counted and seeded at 2 × 10^6 per mL into cell culture dishes. Fresh medium with M-CSF1 was added every 2–3 days.

After 8 days of differentiation (cells adhere to culture dish surface and stretch) BMDMs were harvested with Trypsin/EDTA and seeded at 0.4 to 1 × 10^5 cells/mL depending on the subsequent assays described below (BMDM cell proliferation, phagocytic activity, intracellular ROS production, and gene expression by RNA-seq or qPCR).

For gene expression analysis, BMDMs were stimulated with 100 ng/mL LPS, or with 1 μg/mL Concanavalin A (Con A). After 24 h, RNA was isolated by TRIzol/Chloroform. Intracellular ROS production in BMDMs was determined as previously described[7] using 2′,7′-dichlorodihydrofluorescein diacetate (H_2DCFDA).

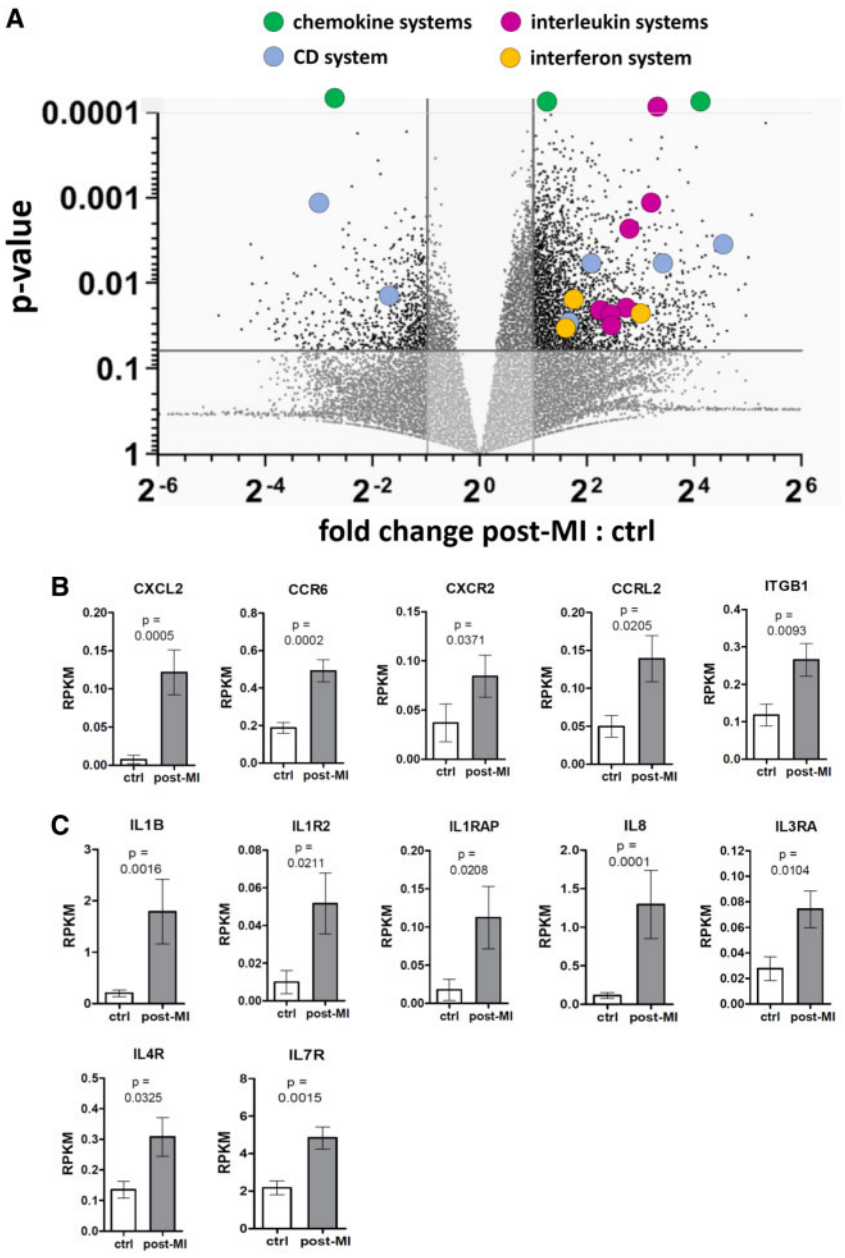

Figure 2 Anomalous immune-related protein expression in post-MI patient PBMCs. (*A*) Volcano plot depicting transcript fold-change post-MI PBMCs ($n = 28$): control PBMCs ($n = 31$) vs. *P*-value. Deregulated coding transcripts from four functional classes are indicated by coloured dots. For each transcript measured, the plot depicts the *P*-values obtained by Student's *t*-test comparing the test cohorts of 28 post-MI patients vs. 31 controls. (*B–E*) Comparison of the most highly deregulated transcripts in post-MI patient vs. control PBMCs encoding chemokines/receptors (*B*), interleukins/receptors (*C*), components of the interferon system (*D*), and immune cell differentiation (CD) antigens + MMP28 + FOXP1 (*E*). To obtain the *P*-values for inter-group comparison of these test cohorts, Student's *t*-test was used. The mean values ± SEM are indicated. The mean ± SEM RPKM values for *all* significantly deregulated lncRNAs and coding transcripts in patients and controls, respectively, are given in Supplementary material online, *Table S3A*. (*F*) ROC analyses comparing the potential of deregulated transcripts to discriminate the test cohorts of 28 post-MI patients vs. 31 controls. The curve to the left encompasses coding transcripts from *Figure 2*, the curve to the right refers to lncRNAs from *Figure 1*.

Analysis of phagocytic activity of BMDMs was performed according to the manufacturer's instructions. As *pHrodo Green Zymosan A Bioparticles (Molecular Probes)* are ingested by phagocytosing cells, the pH decreases and the pH-sensitive dye increases fluorescence. BMDMs were cultured in black 96 wells with or without LPS for 24 h, and for 1 h with 10 μM of the phagocytosis inhibitor Cytochalasin D (Cyto D) (*Cayman Chemical*), respectively. The plate was put on ice for 15 min to synchronize the cells and the medium was replaced with particle suspension. Similar to DCF

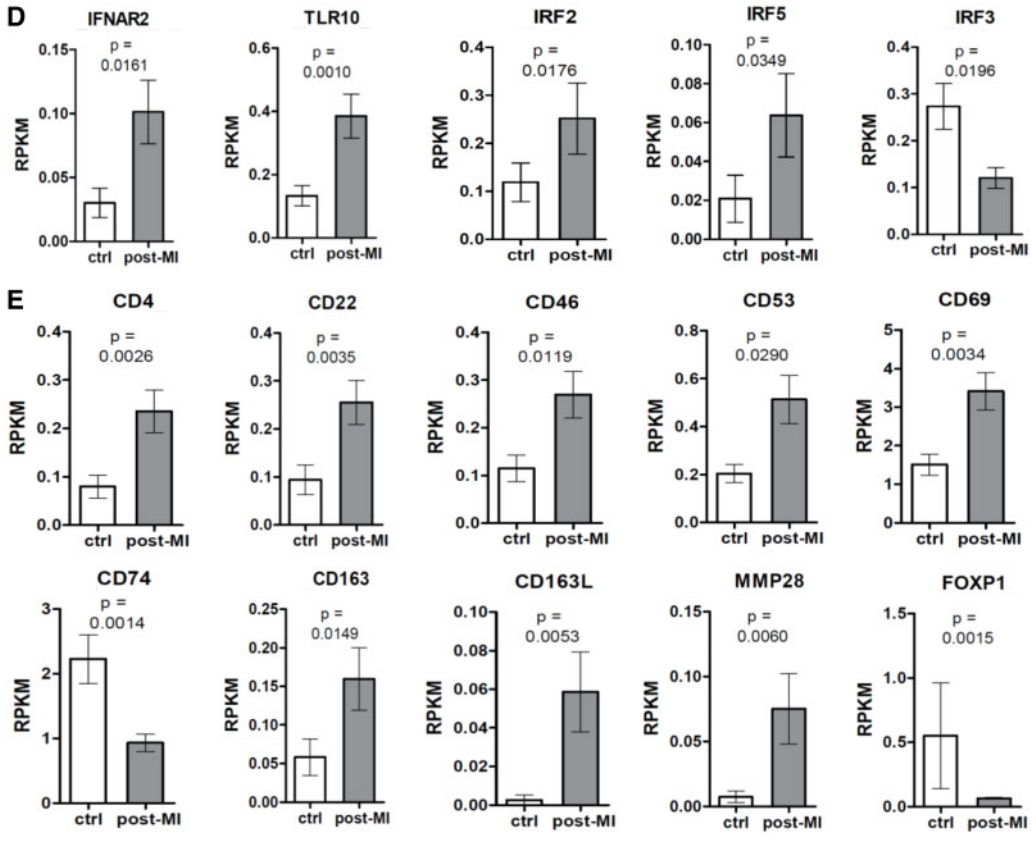

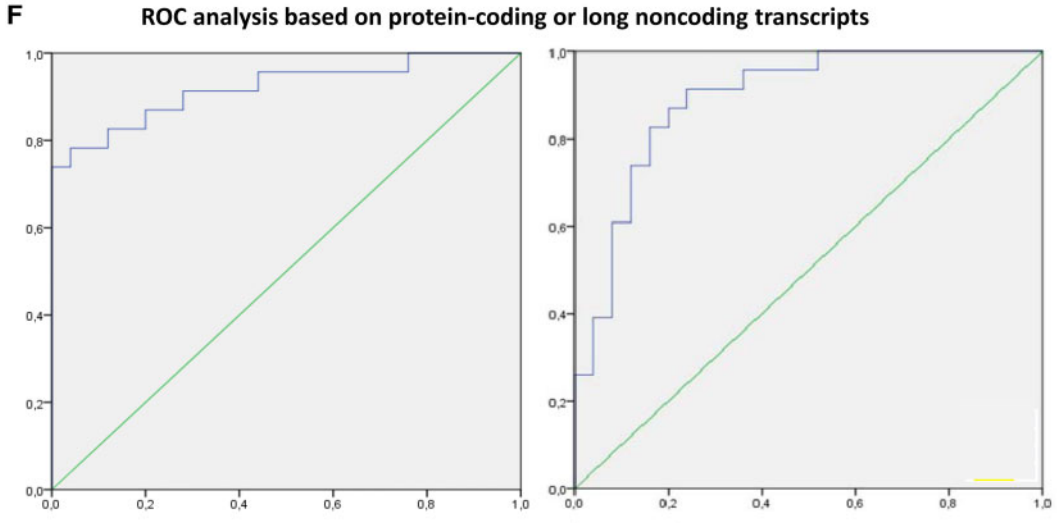

AUC	SE	sign	95% CI lower	95% CI upper
,920	,042	,000	,839	1,000

AUC	SE	sign	95% CI lower	95% CI upper
,882	,047	,000	,789	0.974

Figure 2 Continued.

assay, fluorescence was determined every 10 min (excitation 485 nm, emission 540 nm) at 37°C on a *Tecan* plate reader. Phagocytosis of untreated cells was set to 100%.

The BMDM proliferation assay was conducted as follows: 5×10^4 BMDMs were seeded into clear 96 well plates—one plate for each time point. Proliferation was determined using WST1 reagent (*Sigma-Aldrich*) according to the manufacturer's instructions. Absorbance at 450 nm was measured 2 h after addition of WST1 and incubation at 37°C on a *Tecan* plate reader. Absorbance of WT cells was set to one at each time point.

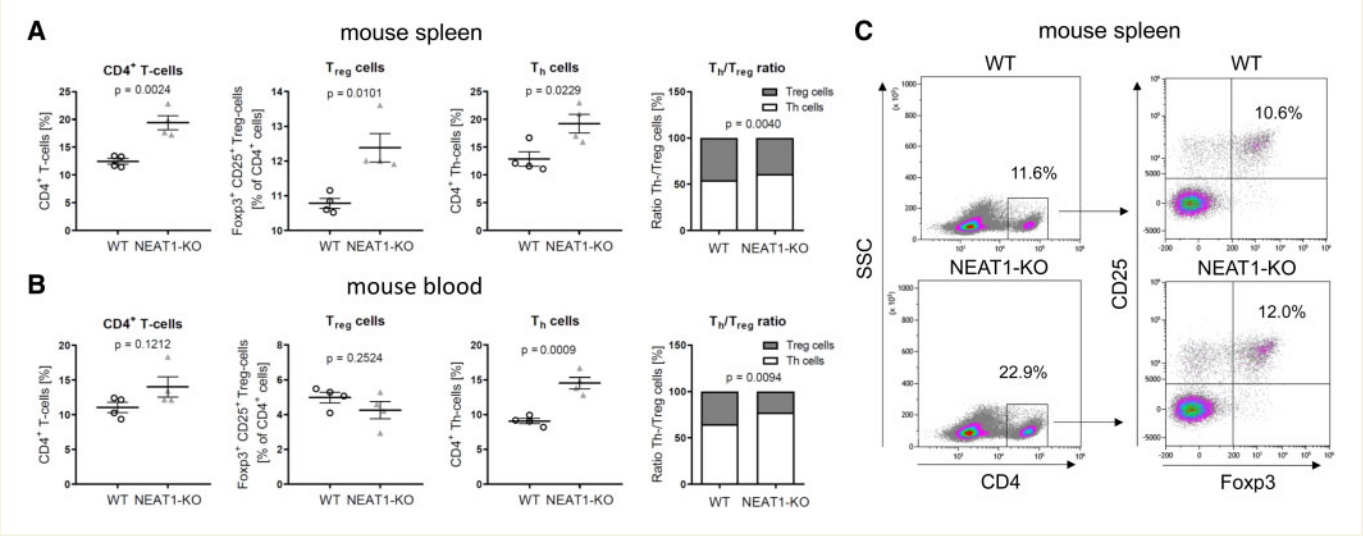

Figure 3 Investigation of splenocytes and T cell populations in *NEAT1*$^{-/-}$ mice. (*A–C*) FACS analysis identified significant differences regarding T cell differentiation in the spleens of *NEAT1*$^{-/-}$ vs. WT mice *in vivo* ($n = 4$ animals per group). There was expansion of T helper (Th) cells ($P = 0.0229$) and T regulatory (Treg) cells ($P = 0.0101$) in the spleens of *NEAT1*$^{-/-}$ mice, with a shift of CD4+ T cell balance (ratio Th/Treg) towards Th cell proliferation both in the spleens ($P = 0.004$) (*A*) and in the circulating blood ($P = 0.0094$) (*B*). To obtain the *P*-values for inter-group comparison, Student's *t*-test was used. The individual measurements and the mean values ± SEM are indicated. (*C*) Specifies the gating strategy for the FACS analyses of T cells in splenocytes. (*D*) Interferon (IFN) γ expression was ≈14-fold higher in unstimulated splenocytes from *NEAT1*$^{-/-}$ mice compared with WT, the largest difference of any transcript level as detected by RNA-seq based mapping (compare Supplementary material online, *Table S4A*). Splenocytes from $n = 4$ animals per group were isolated, total RNA isolated from the cells was pooled for each group, and RNA-seq done on these RNA pools. The resulting mean FPKM values are given in *D* and Supplementary material online, *Table S4A*. (*E*) CBA measurement of six circulating cytokines revealed significantly ($P = 0.0226$) higher IFNγ levels in the sera of *NEAT1*$^{-/-}$ mice ($n = 11$) compared with WT animals ($n = 8$). To obtain the *P*-values for inter-group comparison, Student's *t*-test was used. The individual measurements and mean values ± SEM are indicated. For the five other evaluated cytokines no significant differences were observed (Supplementary material online, *Figure S1B*). (*F*) ROS assays showed ≈3-fold increased ($P < 0.0001$) ROS production by *NEAT1*$^{-/-}$ compared with WT splenocytes under baseline conditions (graph to the left). Neither PMA nor PMA + LPS stimulation significantly increased ROS production by either strain compared with their respective baseline levels (graph to the right). Intra-splenocytic ROS production was measured in $n = 15$ WT and $n = 9$ *NEAT1*$^{-/-}$ separate splenocyte preparations without stimulation (mock), or stimulated with PMA or PMA+LPS, respectively. The graphs depict the individual measurements and means ± SEM of the measured ROS production values for each animal group (WT vs. *NEAT1*$^{-/-}$) under the three different conditions. To obtain the *P*-values for inter-group comparison, Student's *t*-test was used. (*G*) Transcriptome mapping of *NEAT1*$^{-/-}$ splenocytes vs. WT identified major alterations of baseline expression levels (Supplementary material online, *Table S4A*) and regulation upon LPS stimulation (Supplementary material online, *Table S4B*) of multiple immune-related genes including interleukins and their receptors, proteins of early innate immunity and the IFN system, TNF and caspases, and matrix metalloproteinases. (*G*) Expression data for several chemokines and chemokine receptors is summarized. Splenocytes from $n = 4$ animals per group were isolated, treated with LPS vs. saline, then total RNA was isolated from the treated cells and pooled for each group. RNA-seq was done on these RNA pools and the resulting mean FPKM values are given in *G* and Supplementary material online, *Table S4B*. *NEAT1*$^{-/-}$ splenocytes displayed a response to LPS exposure (i.e. down-regulation compared with baseline), which is opposite to the response of WT cells to this treatment. Contrary to this anomalous down-regulation of multiple chemokines and chemokine receptors in *NEAT1*$^{-/-}$ mice, a broad spectrum of small nucleolar RNAs (Snords) became >1000-fold induced in the knockout strain, while remaining unchanged in WT (exemplarily shown in the box for Snord90, further data in Supplementary material online, *Table S4B*).

2.5.2 Murine splenocytes

For the cell culture studies reported in *Figure 3F* and *G*, multiple splenocytes preparation were conducted from a total of $n = 12$ WT and $n = 12$ *NEAT1*$^{-/-}$ mice. Splenocytes were isolated as follows. Mouse spleens were dissected and meshed through 40 µm cell strainers (rinsed with PBS into 50 mL tube). After centrifugation pellet was washed and resuspended in 1 mL ACK lysis buffer (*Invitrogen*) in order to lyse red blood cells. After 5 min at room temperature, cells were washed again and resuspended in 5 mL RPMI 1640 + 10% FCS + 1% P/S.

For analysis of gene expression and regulation by RNA-seq (*Figure 3D* and *G*), the splenocyte preparation were stimulated with 1 or 100 ng/mL LPS, or 0.1 µM phorbol 12-myristate 13-acetate (PMA). After 24 h, RNA was isolated by *TRIZOL*/Chloroform.

Intracellular ROS production in splenocytes (*Figure 3F*) was determined as previously described[7] using 2′,7′-dichlorodihydrofluorescein diacetate (H_2DCFDA).

2.6 Transcriptome mapping of murine splenocytes and macrophages

For the RNA-seq analyses of splenocyte and BMDM transcriptomes in *NEAT1*$^{-/-}$ vs. WT mice, splenocytes and BMDMs from $n = 4$ animals per group were prepared and *ex vivo* separately treated with various agents as described. Total RNA isolated from these separately treated cell preparations by the *TRIZOL*/Chloroform method. RNA integrity was visualized using an *Agilent Bioanalyzer 2100*. Between 160 and 500 ng total RNA was spiked with ERCC (*Thermo Fisher*) and subjected to rRNA removal using the *Low Input Ribominus Eukaryote System V2* kit according to

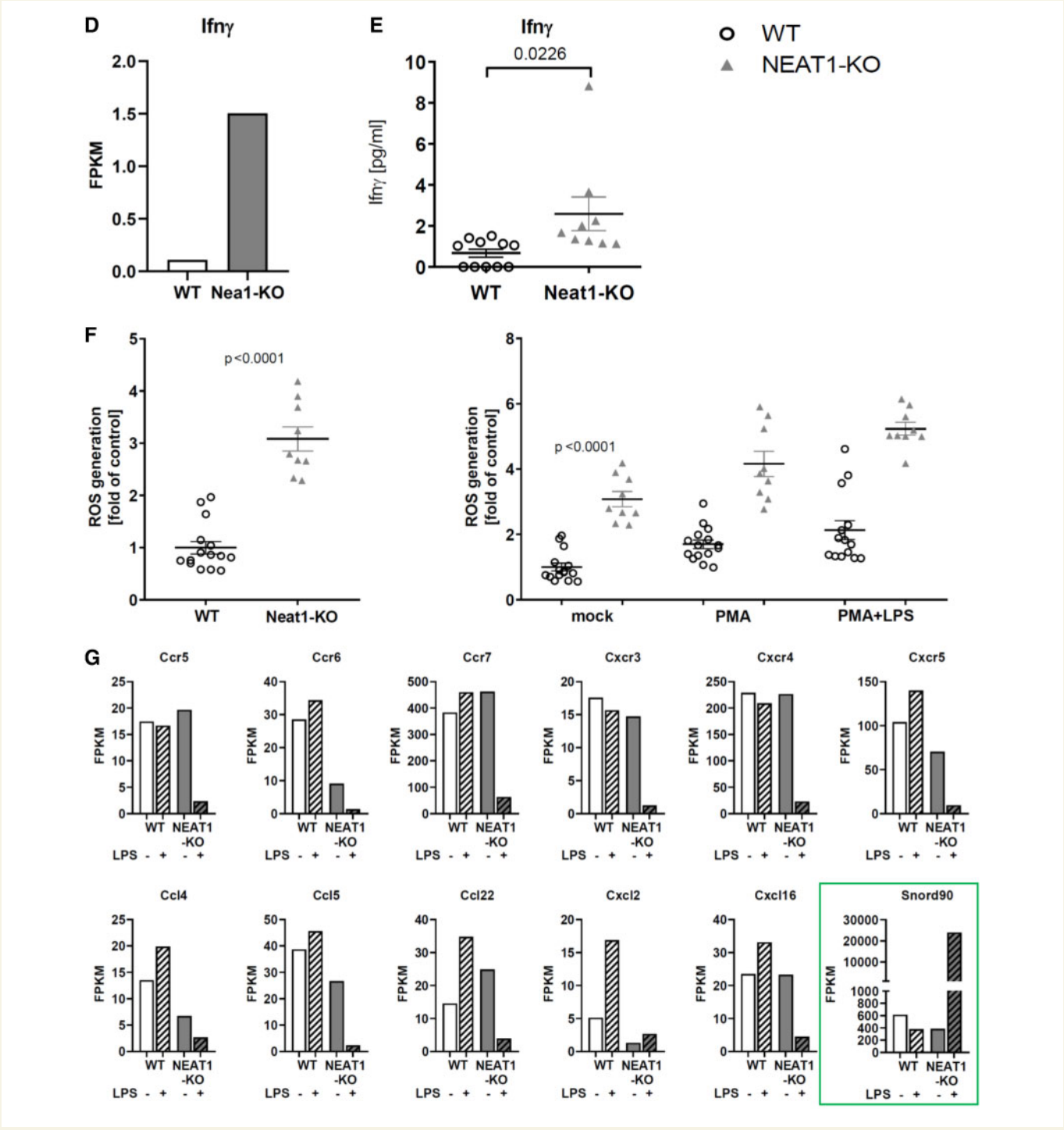

Figure 3 Continued.

the manufacturer's recommendations (*Thermo Fisher*). The RNA was chemically fragmented, barcoded and subject to library preparation using the *Ion Total RNA-Seq Kit V2* protocol according to the manufacturer's recommendations (Thermo Fisher). Libraries were diluted and pooled and further processed using the Ion Chef System, according to the recommended protocols. Libraries loaded onto 540 Ion chips were then sequenced on an *Ion S5 XL Instrument* (*Thermo Fisher*). At least 15×10^6 reads per sample were obtained. Nucleotides were called using standard settings and the reads were mapped to the mouse genome (*GRCm38/mm10*), using the *TMAP* algorithm, also with standard settings. The *htseq-count module* from the software package *HTseq* was used with default parameters to count reads per gene. FPKM (fragments per kilobase transcript per million reads) values were calculated based on the total exon length per gene.

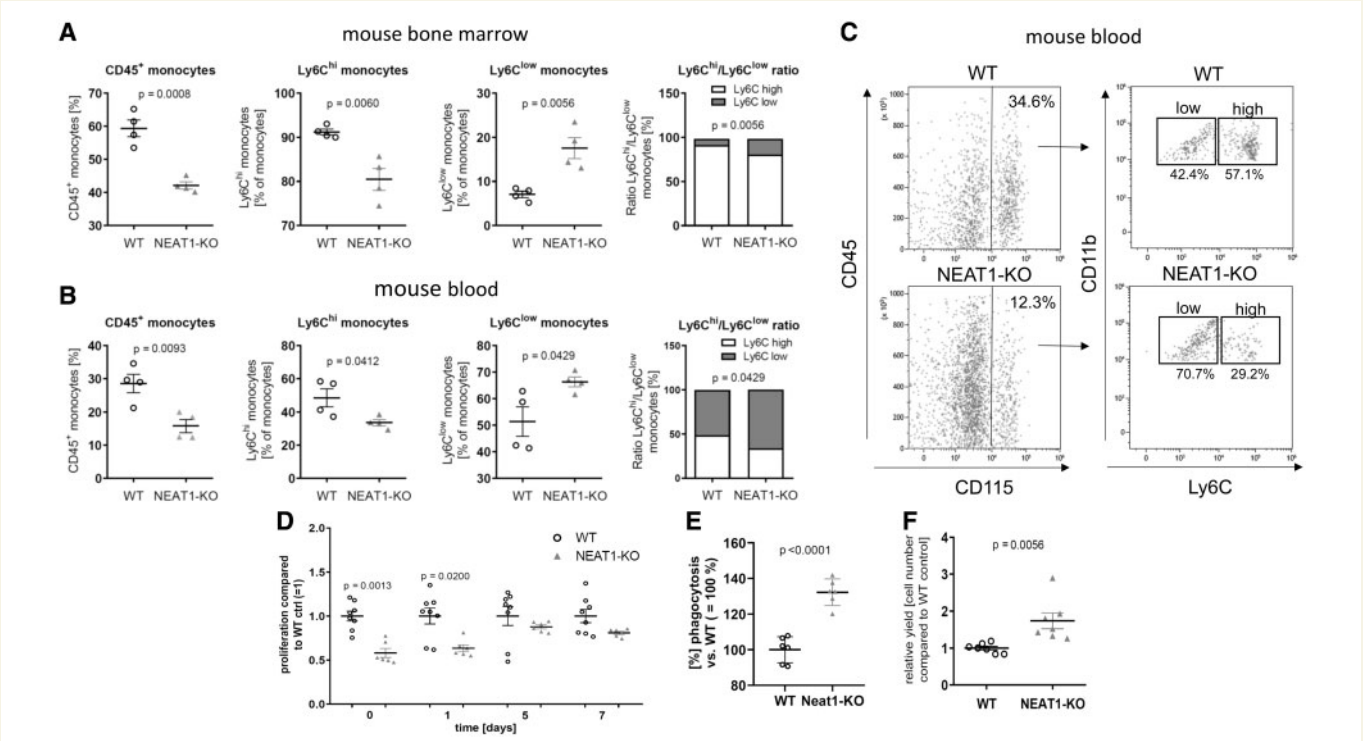

Figure 4 Investigation of the monocyte-macrophage lineage in *NEAT1*$^{-/-}$ mice. (*A–C*) FACS analyses of bone marrow (*A*) and blood (*B*) from *NEAT1*$^{-/-}$ compared with WT mice ($n = 4$ animals per group) identified markedly reduced levels of CD45+ monocytes both in the bone marrow ($P = 0.0008$) and circulating blood ($P = 0.0093$) of *NEAT1*$^{-/-}$ mice. This is reflected by decreased levels of Ly6C^{high} ($P = 0.0060$ in bone marrow; $P = 0.0412$ in blood) and increased levels Ly6C^{low} monocytes in the bone marrow ($P = 0.0056$) and circulating blood ($P = 0.0429$) of *NEAT1*$^{-/-}$ mice. To obtain the *P*-values for inter-group comparison, Student's *t*-test was used. The individual measurements and the mean values ± SEM are indicated. (*C*) The gating strategy for FACS analyses of monocytes in blood is given. The *D–F* summarize several functional anomalies of *NEAT1*$^{-/-}$ BMDMs, which were observed under baseline conditions, while other emerged only upon LPS exposure (*G–I*). (*D*) After *ex vivo* differentiation with M-CSF, *NEAT1*$^{-/-}$ BMDMs displayed lower proliferation rates compared with WT cells (Day 0 after differentiation: $P = 0.0013$, Day 1: 0.0200). This difference vanished with prolonged time of the BMDMs in culture. Cell proliferation was measured in $n = 8$ WT and $n = 6$ *NEAT1*$^{-/-}$ separate BMDM preparations. The graph depicts the individual measurements and means ± SEM of the measured proliferation rates for each animal group (WT vs. *NEAT1*$^{-/-}$) at four different time points (0, 1, 5, and 7 days) after *ex vivo* differentiation with M-CSF. The given *P*-values for inter-group comparison were obtained by Student's *t*-test. (*E*) Baseline phagocytotic activity was measured in $n = 6$ WT and $n = 6$ *NEAT1*$^{-/-}$ separate BMDM preparations. The graph depicts the individual phagocytosis measurements (normalized to WT mean) and the means ± SEM for each animal group (WT vs. *NEAT1*$^{-/-}$) without stimulation (compare *H* for LPS and CytoD stimulation). The given *P*-values for inter-group comparison were obtained by Student's *t*-test. (*F*) The yield of BMDMs obtained after 8 days of *ex vivo* differentiation, from a given number of input bone marrow cells flushed from the femoral cavity of *NEAT1*$^{-/-}$ compared with WT animals, was determined during the preparation of BMDMs from $n = 7$ WT and $n = 7$ *NEAT1*$^{-/-}$ mice. The graph depicts the individual yields (normalized to WT mean) and the means ± SEM for each animal group (WT vs. *NEAT1*). The given *P*-values for inter-group comparison were obtained by Student's *t*-test. The *G–I* display functional anomalies of *NEAT1*$^{-/-}$ BMBMs which emerged upon LPS stimulation. (*G*) *NEAT1*$^{-/-}$ BMDMs responded to LPS with massively increased ($P < 0.0001$) ROS production compared with WT BMVMs (graph to the left). Intracellular ROS production was measured in $n = 8$ WT and $n = 8$ *NEAT1*$^{-/-}$ separate BMDM preparations without stimulation (mock), or stimulated with LPS (100 ng/mL) or ConA (1 µg/mL), respectively. The graph depicts the individual measurements and the means ± SEM of the measured ROS production values for each animal group (WT vs. *NEAT1*$^{-/-}$) under the three different conditions. To obtain the *P*-values for inter-group comparison, Student's *t*-test was used. NOS2 expression was significantly increased in *NEAT1*$^{-/-}$ vs. WT mice (graph to the right). NOS2 mRNA was quantitated by pPCR in $n = 6$ WT and $n = 6$ *NEAT1*$^{-/-}$ separate BMDM preparations without stimulation (mock), or stimulated with LPS or ConA, respectively. The graph depicts the individual measurements and the means ± SEM for each animal group (WT vs. *NEAT1*$^{-/-}$), with >1000-fold induction by LPS (100 ng/mL) in both groups relative to baseline. The given *P*-values for inter-group comparison were obtained by Student's *t*-test. (*H*) *NEAT1*$^{-/-}$ cells displayed higher baseline phagocytosis activity as shown in *E*. However, the response *NEAT1*$^{-/-}$ BMDMs to LPS was attenuated compared with WT cells. In the graph, LPS-stimulated phagocytosis of either strain is compared with their respective baseline ('mock') activity set to 100%. The graph depicts the individual phagocytosis measurements (normalized to WT mean) and the means ± SEM for each animal group (WT vs. *NEAT1*$^{-/-}$) without stimulation (mock), upon stimulation with LPS at 100 ng/mL, or in the presence of the phagocytosis inhibitor cytochalasin D (Cyto D) at 10 µM concentration. The given *P*-values for inter-group comparison were obtained by Student's *t*-test. (*I*) RNA-seq detected multiple anomalies in *NEAT1*$^{-/-}$ BMDMs under baseline conditions (*Figure 4I*, Supplementary material online, *Table S5A*) and upon stimulation with LPS (Supplementary material online, *Table S5B*). BMDMs from $n = 4$ animals per group were isolated, treated with LPS vs. saline, then total RNA was isolated from the treated cells and pooled for each group. RNA-seq was then conducted on these RNA pools and the resulting mean FPKM values are presented in this panel and Supplementary material online, *Table S5A* and *B*. Partially overlapping with the transcriptional changes observed in *NEAT1*$^{-/-}$ splenocytes, there was deregulation of several CC and CXC chemokines and chemokine receptors in *NEAT1*$^{-/-}$ BMDMs at baseline. Upon LPS stimulation, deregulation of these systems persisted (Supplementary material online, *Table S5B*).

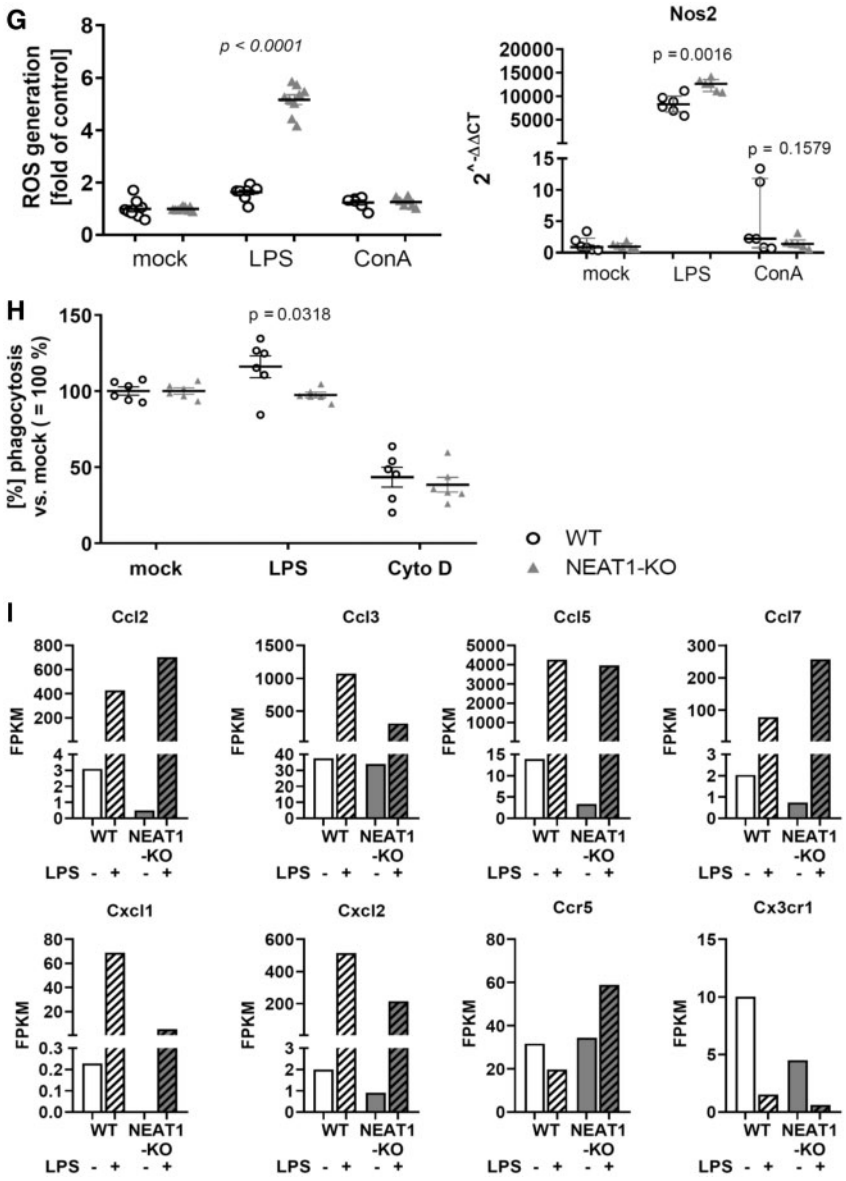

Figure 4 Continued.

2.7 Quantitative RT-PCR

cDNA transcription and qPCR were conducted using standard methods, the PCR primers used are given in the Supplementary material online. Reference gene was HPRT unless indicated otherwise. Expression levels measured by qPCR were quantified as delta-delta-C_t values, determined by the C_t value of a candidate RNA minus the C_t of the reference gene.

2.8 FACS analyses on murine blood, spleen, and bone marrow

Blood samples were from $n = 4$ WT and $n = 4$ *NEAT1*$^{-/-}$ mice was collected by cardiac puncture using EDTA-coated syringes. Whole blood (100 µL) or bone marrow (BM) cell suspension was incubated with antibodies for 20 min at room temperature in the dark. BM cells were collected from both tibiae of mice by flushing the BM with Dulbecco's PBS. Harvested cells were filtered through a 70 mm cell strainer and washed with PBS. Erythrocytes from all samples were lysed with red blood cell (RBC) lysis buffer. BM cell suspension was incubated with antibodies for 20 min at room temperature in the dark.

Monocytes were identified after doublet exclusion as CD45 positive and CD115 positive and further selected by highly positive expression of CD11b, a marker of dendritic cells, monocytes and granulocytes, shown in the CD11b/Ly6C plot. Monocytes were further classified according to Ly6C expression. The following antibodies were used: anti-mouse Ly6C (Gr1) PerCp/Cy5.5 Antibody (*Biolegend, B194615*); anti-mouse CD45

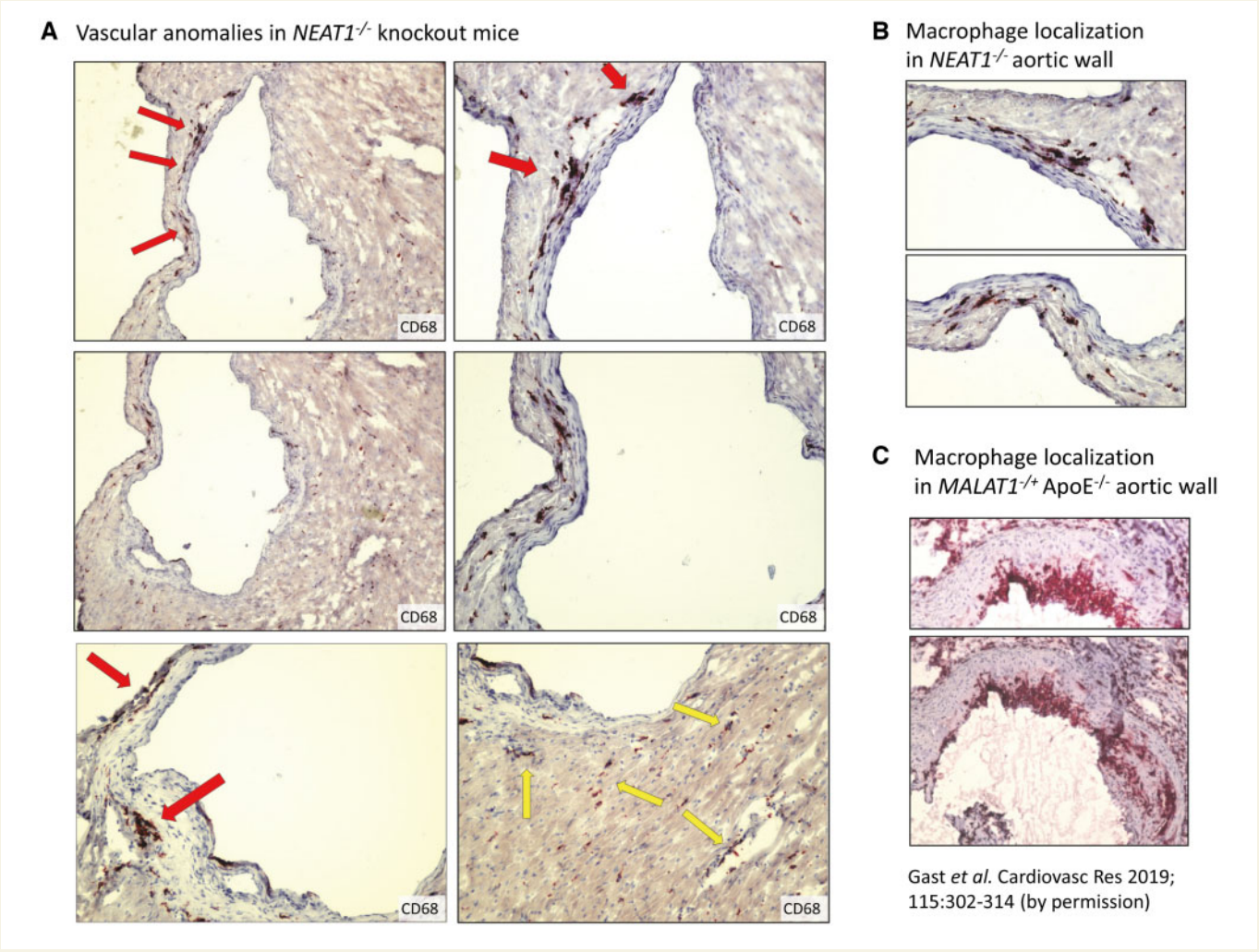

Figure 5 Histological and immunohistological studies in *NEAT1*$^{-/-}$ mice. First, cryosection were prepared from the aortic roots of $n = 4$ WT and $n = 4$ *NEAT1*$^{-/-}$ mice for HE staining (not shown) and CD68+ cell immunhistochemistry as depicted in *A* and *B*. *NEAT1*$^{-/-}$ mice displayed anomalous CD68+ monocyte-macrophage infiltration (red arrows) of the aortic wall, but also in myocardial tissue (yellow arrows). Quantitation of CD68+ monocyte-macrophage infiltration is given in Supplementary material online, *Figure S2*. The CD68+ cell localization observed in *NEAT1*$^{-/-}$ mice (*A* and *B*) was clearly distinct from that previously observed in *MALAT1*$^{-/-}$ ApoE$^{-/-}$ mice (*C*) who developed atherosclerosis even on normal diet. In contrast, the *NEAT1*$^{-/-}$ mice now studied displayed no evidence of even incipient atherosclerosis when kept on normal diet (Oil Red stainings not shown). Whereas the cryosections allowed quantitative evaluation of aortic CD68+ cell infiltration, they yielded suboptimal tissue section quality with regard to the myocardium. To investigate myocardial architecture and histopathology in more detail, we therefore prepared the hearts of another $n = 4$ WT and $n = 4$ *NEAT1*$^{-/-}$ mice for formalin fixation and paraffin embedding. Myocardial paraffin sections were of significantly higher quality thus enabling more detailed histological (haematoxylin–eosin, trichrome) and immunohistochemical (F4/80, CD4, CD8, ADRP) studies of *NEAT1*$^{-/-}$ vs. WT myocardium as shown in *Figure 5D* and *E* and Supplementary material online, *Figure S3A–E*. Beyond the elevated myocardial CD68+ cell infiltration already visible in cryosection, the studies on paraffin sections provided unexpected evidence of more extensive myocardial injury in two of the eight *NEAT1*$^{-/-}$ mice investigated. In conjunction with the observed systemic inflammation with elevated IFN-γ levels in *NEAT1*$^{-/-}$ mice, this strongly suggests future systematic histopathological investigation of multiple organs in these animals which so far have not been routinely preserved for analysis. (*D*) HE stainings with extensive remodelling of the left ventricular wall visible at low resolution (D1), substitution of normal myocardium by adipose-like tissue (D2 and D3), and localized clusters of siderophages near the area of the extensive remodelling (D4 and D5) are shown. (*E*) Further histological (EvG—Elastica van Gieson) and immunohistological characterization documenting (E2 and 3) that the adipose-like tissue does in fact stain positive for ADRP, a member of the perilipin protein family which coat intracellular lipid storage droplets and are involved in the development and maintenance of adipose tissue is shown. EvG staining (E4) did not reveal significantly increased connective tissue formation in or around the injured area. Overall, double staining for CD4+ and CD8+ T cells (E1) did not show significantly increased CD4+ (brown) or CD8+ (red) cell infiltration of the myocardium compared with WT. E6 shows a CD4+ cell within a vessel, E7 a CD8+ cell within the myocardium (red arrows) (for further histological and immunohistological stainings see Supplementary material online, *Figure S3A–E*).

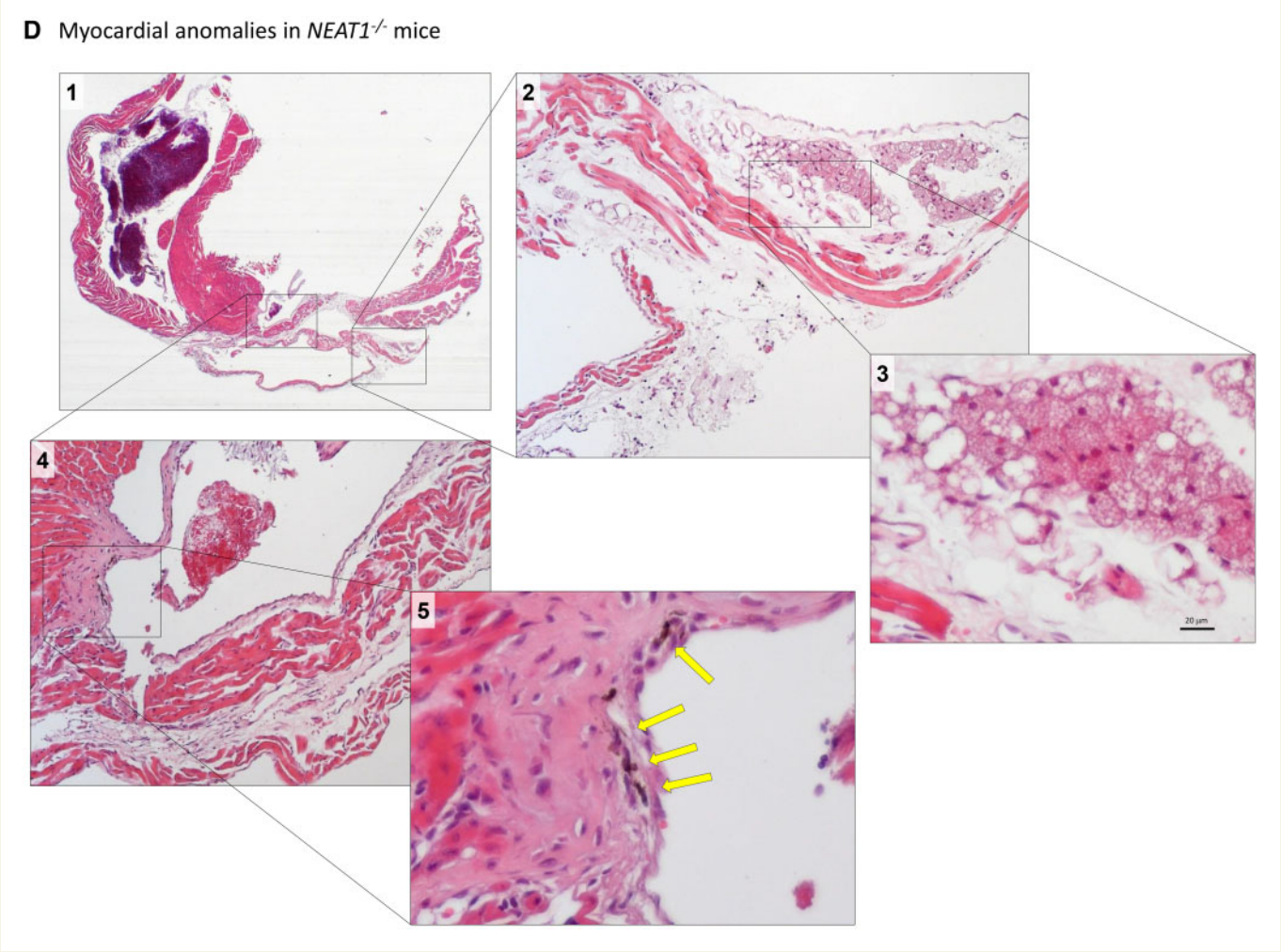

Figure 5 Continued.

PE/Cy7 Antibody (*Biolegend, B205174*); anti-mouse CD115 AF488 Antibody (*Biolegend, B180483*); anti-mouse CD11b BV711 Antibody (*Biolegend, B203911*).

For analysis of $CD4^+$ T cells, cells were stimulated for 4 h with ionomycin (1 µM) and PMA (50 ng/mL) in the presence of monensin (2 µM) and stained for CD4 (*RM4-5, eBioscience*), intracellular IL-17A (*TC11-18H10 BD Pharmingen*), and interferon γ (IFNγ) (*B27 BD Pharmingen*). A fixable viability dye *eFluor™780* (0.2 µL/test) was used to exclude dead cells. Treg cells were stained by using the FoxP3+ Treg staining (FJK-16S, eBioscience) CD25 (Invitrogen).

2.9 Histology and immunohistology of murine organs

Heart and aorta were prepared from $n = 4$ WT and $n = 4$ *NEAT1*$^{-/-}$ mice to be shock-frozen for subsequent cryosections, HE staining and C68 immunhistochemistry as described in *Figure 5A* and *B* and quantitated in Supplementary material online, *Figure S2*. Cryosections allowed quantitative evaluation of CD68+ cell infiltration of the aortae, but produced suboptimal tissue section quality with regard to the myocardium. To investigate myocardial architecture and histopathology in more detail, we therefore prepared hearts and aortae from another $n = 4$ WT and $n = 4$ *NEAT1*$^{-/-}$ mice for formalin fixation and paraffin embedding. Myocardial tissue sections were significantly better quality enabling the extended histological (haematoxylin–eosin, trichrome) and immunohistochemical (F4/80, Cd4, CD8, ADRP) studies of *NEAT1*$^{-/-}$ vs. WT myocardium (*Figure 5D* and *E* and Supplementary material online, *Figure S3A–E*).

2.10 Measurement of circulating cytokines

Serum samples from $n = 11$ WT and $n = 9$ *NEAT1*$^{-/-}$ mice were tested for IFNγ, tumour necrosis factor (TNF), IL6, MCP1, IL10, and IL12p70 by use of *Mouse Inflammation Cytometric Bead Assay* (CBA) (*BD Biosciences, Heidelberg, Germany*) on a *FACS CantoII flow cytometer* (*BD Biosciences*) according to the manufacturer's protocol.[8]

2.11 Statistical analyses

Statistical data analyses were done using *IBM SPSS Statistics 24* or *GraphPad* software. Descriptive statistics include absolute and relative frequencies for categorical variables and mean and standard deviation, median, and range for quantitative measurements. For inter-group

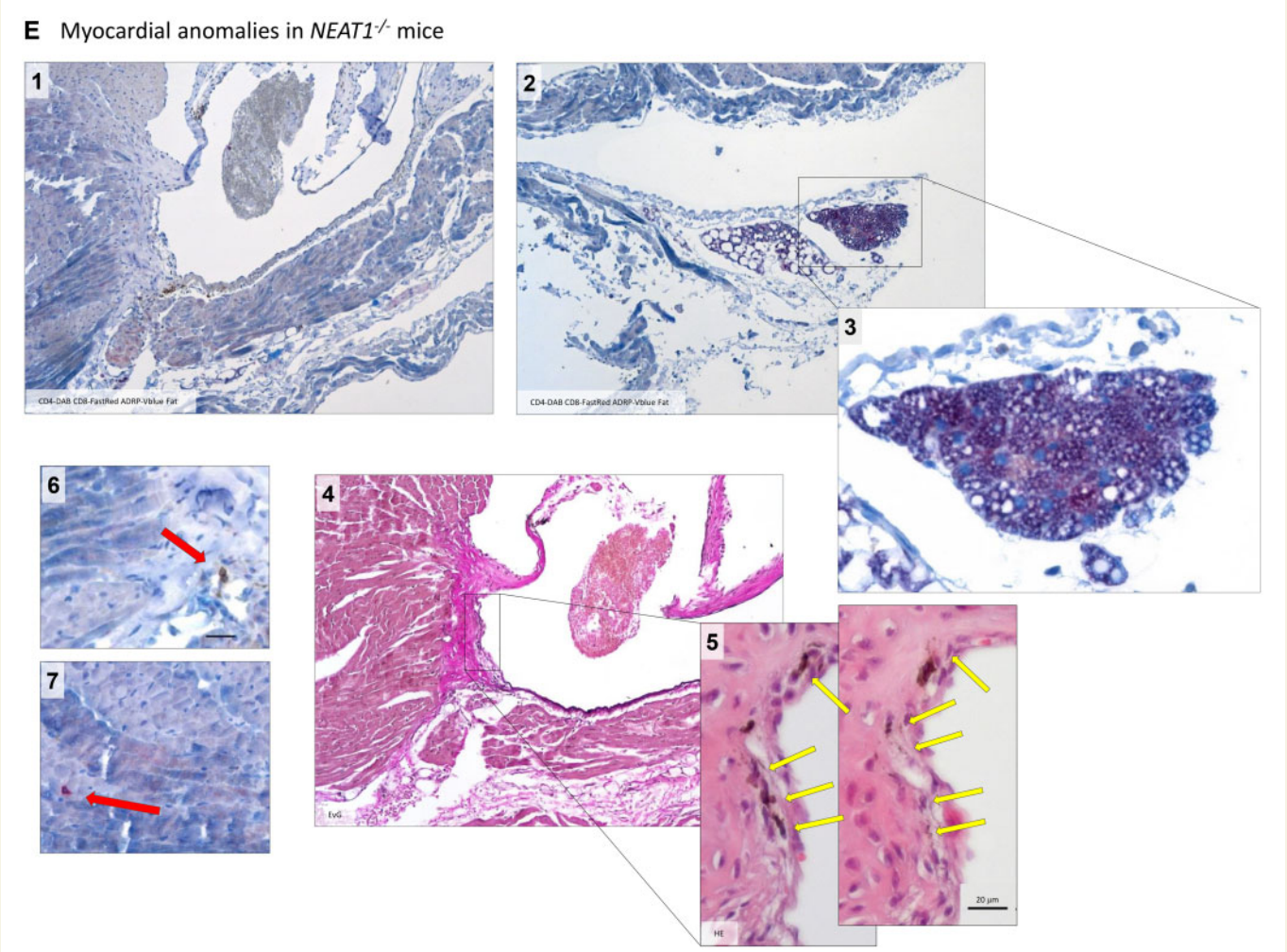

Figure 5 Continued.

comparisons Student's *t*-test or the χ^2 test was used for quantitative or categorical variables, respectively. *P*-values ≤0.05 are considered significant, and no Bonferroni adjustment has been performed.

Adjustment for potential confounders concerning the association between *NEAT1* levels and patient group (*Table 1*) was performed using a multiple linear regression with *NEAT1* levels as the independent variable and patient group, the intake of statin, left ventricular ejection fraction (LVEF), low-density lipoprotein (LDL), high-density lipoprotein (HDL), age, diabetes, and smoking as the independent variables. Due to the skewed distribution of *NEAT1* levels, regression analysis was preceded by a logarithmic transformation.

Diagnostic accuracy was evaluated by uni- and multivariate receiver operating characteristic (ROC) analysis, and area under the curves (AUCs) with 95% confidence intervals are presented. For multivariate ROC, the score derived from multiple logistic regression analysis was included into the ROC model (*Figure 2F*).

Further details on the methods and any associated references, as well as Supplementary material online, *Figures* are available in the Supplementary material online.

3. Results

3.1 Circulating immune cell transcriptomes in early onset MI patients

A cell culture study had suggested immunoregulatory functions of *NEAT1 in vitro*.[3] We therefore carried out an initial qPCR-based prescreening of *NEAT1* and few selected other transcripts in PBMCs from post-MI patients vs. healthy controls (Supplementary material online, *Table S2*). This selective prescreening detected significant down-regulation of *NEAT1* and prompted subsequent RNA-seq to obtain comprehensive non-selective immune cell transcriptomes. Individual RNA-seq was conducted on PBMCs from 28 post-MI patients with a history of MI at age ≤50 years and stable disease ≥3 months before study participation, and on PBMCs from 31 healthy individuals without manifest cardiovascular disease or family history of MI as controls.

The results of this comprehensive screening for lncRNAs and protein-codingn transcripts are summarized in *Figures 1* and *2*, respectively. The rationale of our lncRNA selection process (*Figure 1A–C*), and for our final focus upon *NEAT1*, encompasses four steps. First, there were only

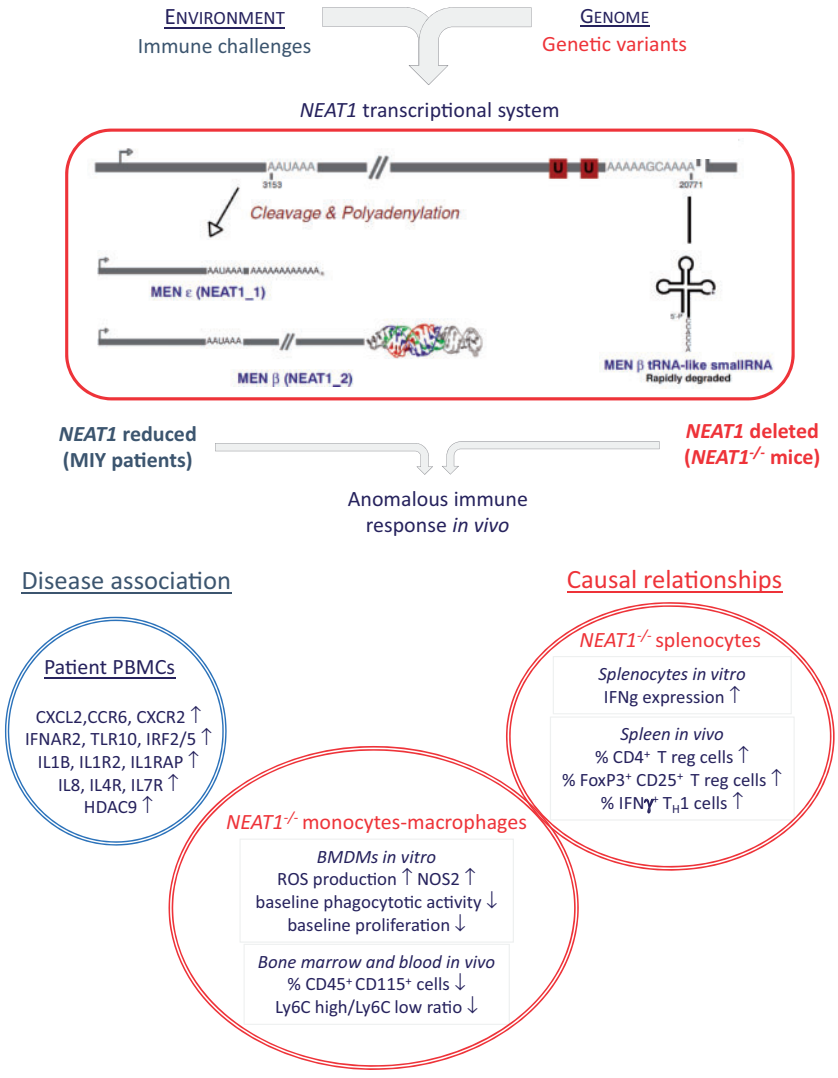

Figure 6 Summary of clinical and experimental data. Individual RNA-seq on PBMCs from patients with a history of MI at age ≤50 years and stable disease ≥3 months before study participation, revealed deregulated protein-coding transcripts and lncRNAs in PBMCs from these patients vs. controls. Among these lncRNAs *NEAT1* was the most highly expressed lncRNA, and the only one significantly suppressed in patients. Multivariate statistical analysis of validation cohorts indicated that the PBMC *NEAT1* levels were influenced by post-MI status independent of statin intake, LVEF, LDL or HDL cholesterol, or age. Prompted by these clinical findings, *NEAT1*$^{-/-}$ mice were investigated as a model of *NEAT1* deficiency to test if *NEAT1* depletion might cause immune system dysfunction. In fact, RNA-seq of *NEAT1*$^{-/-}$ splenocytes identified altered baseline expression and LPS response of chemokines/receptors, innate immunity genes, TNF, and caspases, and increased ROS production under baseline conditions. *NEAT1*$^{-/-}$ spleen displayed anomalous Treg and Th cell differentiation. *NEAT1*$^{-/-}$ BMDMs displayed grossly altered transcriptomes with disturbed chemokine/chemokine receptor expression, increased baseline phagocytosis ($P < 0.0001$) and attenuated proliferation (Day 0: $P = 0.0013$; Day 1: $P = 0.02$). *NEAT1*$^{-/-}$ BMDMs responded to LPS with increased ROS production ($P < 0.0001$), NOS2 mRNA expression ($P = 0.0016$), and disturbed phagocytic activity ($P = 0.0318$). Monocyte-macrophage lineage differentiation was anomalous in *NEAT1*$^{-/-}$ bone marrow and blood. Finally, *NEAT1*$^{-/-}$ mice displayed anomalous aortic CD68^{+} cell infiltration and there was evidence of myocardial inflammation which could lead to severe and potentially life-threatening structural damage in some of these mice.

relatively few significantly deregulated lncRNAs (Supplementary material online, *Table S3A*). Second, *NEAT1* was the only lncRNA significantly down-regulated post-MI (*Figure 1B* and *C*). Third, among lncRNAs with known immunoregulatory functions (Supplementary material online, *Table S1*) *NEAT1* is by far the most highly expressed deregulated lncRNA post-MI (*Figure 1D*). Fourth, *NEAT1* is the only one for which a genetic animal model is available. A volcano plot with deregulated lncRNAs marked by red dots (*Figure 1A*) visualizes the fact that only rather few lncRNAs are deregulated, whereas the far overwhelming number of all lncRNAs detected by RNA-seq are 'stably' expressed in post-MI vs. control PBMCs. When lncRNAs with immunoregulatory functions (Supplementary material online, *Table S1*) are considered, those detected by the RNA-seq in PBMCs display a very broad range of expression levels, with *NEAT1* ranking second after *MALAT1* which is not deregulated, however (*Figure 1D*). *NEAT1* expression was ≈10-fold higher than the next-highest expressed lncRNA with immunoregulatory

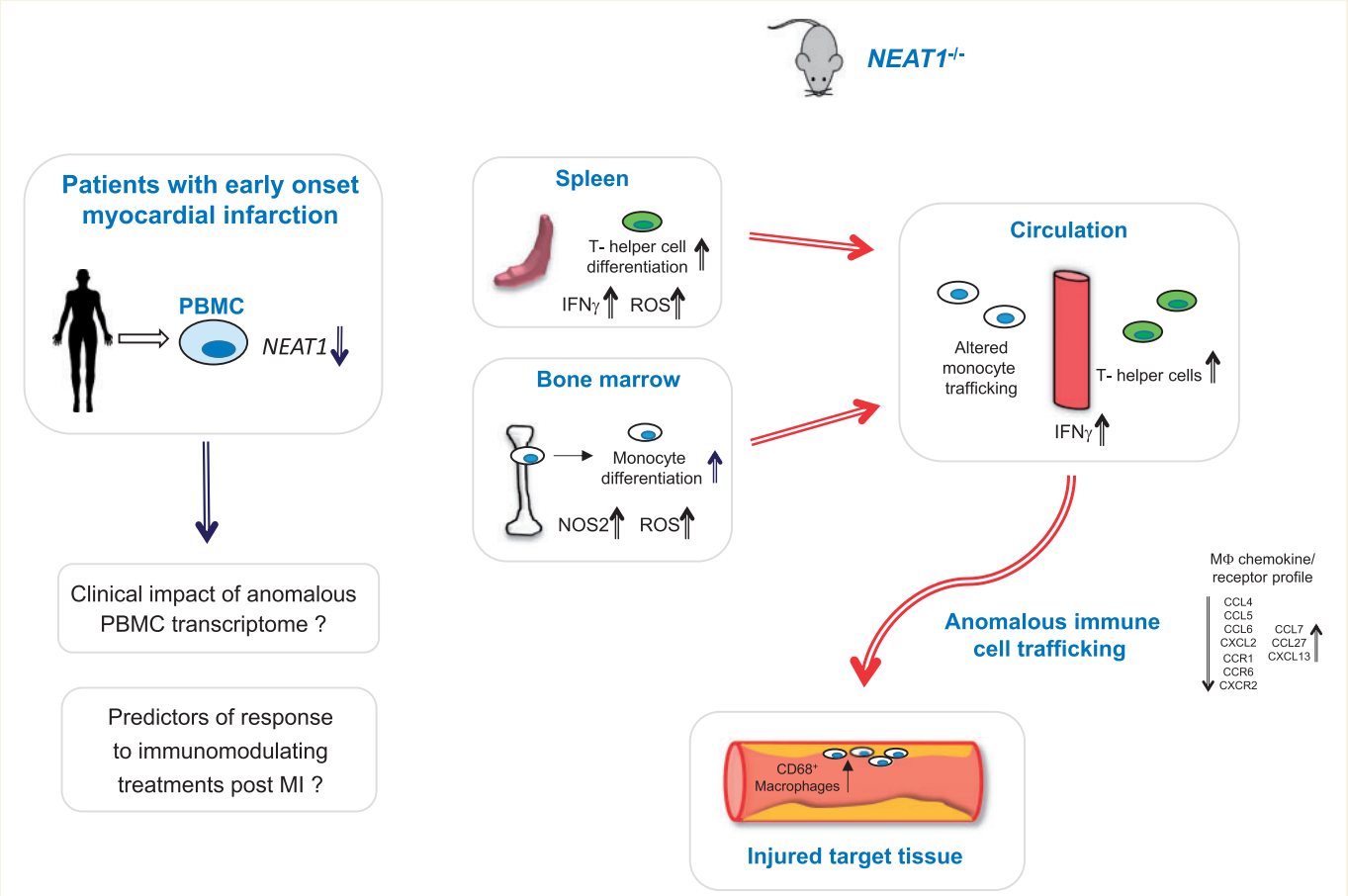

Figure 7 Working model and translational aspects. The animal model and cell culture data support a working model which encompasses disturbances in bone marrow, spleen, and blood circulation of the *NEAT1* deficient mice. In the spleen, there is anomalous T cell differentiation leading to increased circulation of Th cells. Splenocytic IFNγ expression and ROS production is increased even under baseline conditions. There is anomalous monocyte-macrophage differentiation in the bone marrow, and *NEAT1*$^{-/-}$ macrophages display enhanced ROS production and NOS2 expression as well as increased phagocytosis. Once *NEAT1*-deficient cells enter the circulation, their anomalous chemokine/receptor expression should affect their trafficking and may in part explain the histological findings (*Figure 5*). Of note, this 'baseline' scenario describes the situation in animals *not* exposed to external immunological stress. Preliminary insight from our *NEAT1*$^{-/+}$ ApoE$^{-/-}$ strain suggests that even heterozygous *NEAT1* deficiency leads to systemic inflammation with high IFNγ levels upon high cholesterol challenge (Supplementary material online, *Figure S3A*). Future work has to clarify which other disease models may be tolerated by the fragile *NEAT1*$^{-/-}$ strain, and which further insights they may provide regarding the *NEAT1* system. Independent of results from future experimental work, the clinical data already document that *NEAT1* is a significant novel component of a PBMC-based immunoregulatory network remaining markedly 'out-of-balance' post-MI despite standard therapy.

functions (NeST) and the only one suppressed post-MI, while significant up-regulation was observed for seven lncRNAs of unknown function (*Figure 1C*). *NEAT1* suppression first observed in the test cohorts was subsequently confirmed ($P < 0.0001$) by qPCR in validation cohorts of 106 post-MI patients vs. 85 controls (*Figure 1B*).

To assess whether the deregulated lncRNAs are differentially expressed in normal PBMCs, we conducted RNA-seq of RNA pools from five immune cell subpopulations (*Figure 1E*). First, FACS sorting of PBMCs from three healthy individuals was performed, followed by RNA extraction from the respective immune cell subtypes. Subtype RNAs from all three individuals were then pooled and RNA-seq done on these RNA pools. Strikingly differential expression of the deregulated lncRNAs (*Figure 1B* and *C*) was observed in these normal PBMC subpopulations (*Figure 1E*). *NEAT1* as well as LINC00211 were highly enriched in monocytes, distinct from the subtype-related expression of the others (*Figure 1F*).

Multivariate statistical analysis revealed that the *NEAT1* levels were determined by post-MI status, independent of statin intake, LVEF, LDL or HDL cholesterol, age, diabetes, and smoking (*Table 1*).

In addition to these lncRNAs, further anomalies encompassed important immunoregulatory coding genes (*Figure 2*). Our selection process for protein-coding transcripts of particular immunological interest (*Figure 2A–E*) started with the entire set of differentially expressed genes (Supplementary material online, *Table S3A*). We then selected top differentially expressed genes according to functional classes relevant to immune system functions (Supplementary material online, *Table S3B*). *Figure 2A* displays key transcripts from functional classes colour-coded upon a volcano plot of all

Table 1 Multivariate statistical analysis of validation cohorts

Validation cohorts of post-MI patients vs. controls						
	Post-MI $n = 106$			CONT $n = 85$		
	Mean	Median	SD	Mean	Median	SD
Age (years)	45.16	44.50	4.74	45.13	45.00	4.82
LVEF (%)	56.15	57.48	10.40	64.23	63.79	5.49
LDL (mg/dL)	102.95	99.50	37.43	139.92	137.00	32.53
HDL (mg/dL)	45.23	42.50	12.82	51.82	51.00	12.66
NEAT1	20.78	14.75	16.34	40.01	33.04	34.04
Male (%)	106 (100)			85 (100)		
Smoking (%)	29 (27.3)			23 (27.1)		
Diabetes (%)	8 (7.5)			2 (2.3)		
Statin (%)	96 (90.6)			1 (1.2)		

Multiple linear regression analysis of determinants of *NEAT1* in human PBMCs					
Coefficients[a]					
	Unstandardized coefficients		Standardized coefficients		
	B	Standard error	Beta	t	Significance
Group	-0.806	0.240	-0.471	-3.361	0.001
Statin	0.099	0.256	0.058	0.389	0.698
EF	-0.001	0.007	-0.016	-0.214	0.831
LDL	0.002	0.002	0.072	0.906	0.366
HDL	-0.006	0.005	-0.090	-1.291	0.198
Age	-0.015	0.012	-0.084	-1.202	0.231

Model after stepwise selection					
Coefficients[a]					
	Unstandardized coefficients		Standardized coefficients		
	B	Standard error	Beta	t	Significance
Group	-0.725	0.113	-0.424	-6.433	0.000

Multivariate statistical analysis of the validation cohorts showed that the NEAT1 levels were determined by the post-MI status, independent of statin intake, LVEF, LDL or HDL cholesterol levels, age, diabetes, and smoking.
[a]Dependent variable: NEAT1.

deregulated transcripts, illustrating that the individual transcripts shown in *Figure 2B–E* are clearly outliers. To facilitate comparison of these human PBMC data with the experimental results on splenocytes and macrophages from *NEAT1*$^{-/-}$ mice (*Figures 3* and *4*), the same classification is kept across all figures.

The IL1β system constitutes a therapeutic target of major current interest[9–13] and is highly up-regulated (IL1B, IL1R2, IL1RAP) in post-MI PBMCs. Interleukin (IL) 8 is highly induced compared with very low expression in control PBMCs, and known to be increased in serum of patients with cerebro-cardiovascular events.[14] IL3 receptor α (IL3RA),[15] IL7 receptor (IL7R),[16] and chemokine receptor CCR6,[17] all of which are strongly induced, are known to influence immune cell migration in atherosclerosis. Chemokine receptors CXCR2[18] and CCRL2[19] were likewise induced, and CXCL2[20] commonly undetectable in controls was robustly expressed in post-MI PBMCs. Interferon (IFN) α and β receptor subunit 2 (IFNAR2)[21] and TLR10[22] were induced, and IFN regulatory factors were deregulated.[23] While we have not performed FACS analyses of post-MI PBMCs, several *Clusters of Differentiation* (CD) antigens were deregulated at the transcriptional level: CD4, CD22, CD46, CD 53, CD163, and MMP28 were induced, while CD74 and FOXP1 transcription were suppressed (further references[24] in the Supplementary material online).

ROC analysis (*Figure 2F*) to discriminate post-MI patients vs. controls yielded an AUC of 0.920 ± 0.042 [95% confidence interval (CI) 0.839–1.000] ($P < 0.001$) based on protein-coding transcripts (*Figure 2*), whereas deregulated lncRNAs (*Figure 1*) yielded an AUC of 0.882 ± 0.047 (95% CI 0.789–0.974) ($P < 0.001$).

3.2 Anomalous immune system regulation in *NEAT1*$^{-/-}$ mice

As a first step towards mechanistic dissection of the anomalous transcriptomes of post-MI patient PBMC, we used a *NEAT1*$^{-/-}$ mouse model[5,6] to evaluate whether isolated genetic *NEAT1* deficiency might cause dysfunction of the immune system. The choice of *NEAT1* was obvious, as the most highly expressed deregulated lncRNA in human post-MI

PBMCs, for which a genetic animal model and detailed information regarding its post-transcriptional processing are available.[5,25–27] For the other lncRNAs deregulated in the patient PBMCs there is currently no such information.

3.3 Investigation of *NEAT1*$^{-/-}$ splenocytes

3.3.1 Anomalous T cell differentiation and expansion in *NEAT1* deficient mice *in vivo*

FACS analysis identified significant differences regarding T cell differentiation in the spleens of *NEAT1*$^{-/-}$ mice vs. WT mice *in vivo* (*Figure 3A–C*), in addition to alterations of the monocyte-macrophage lineage in blood and bone marrow from *NEAT1*$^{-/-}$ vs. WT mice (*Figure 4A–C*). In particular, we observed expansion of T helper (Th) cells ($P = 0.0229$) and of immune-modulating T regulatory (Treg) cells ($P = 0.0101$) in the spleens of *NEAT1*$^{-/-}$ mice, with a shift of CD4+ T cell balance towards Th cell proliferation both in the spleens ($P = 0.004$) and in the circulating blood ($P = 0.0094$). These results support a crucial function of *NEAT1* in regulating cellular processes within the adaptive immune system.

3.3.2 Transcriptome and ROS production of *NEAT1*$^{-/-}$ splenocytes *ex vivo*

Regarding the interferon system, IFNγ expression level was ≈14-fold higher in unstimulated splenocytes from *NEAT1*$^{-/-}$ mice compared with WT cells, the largest difference of any transcript level as detected by RNA-seq based mapping (*Figure 3D* and Supplementary material online, *Table S4A*). Of note, the measurement of six circulating cytokines revealed significantly ($P = 0.0226$) higher IFN-γ levels in the sera of *NEAT1*$^{-/-}$ mice compared with WT (*Figure 3E*). For the other evaluated cytokines no significant differences were observed (Supplementary material online, *Figure S1B*).

ROS assays showed significantly ($P < 0.0001$) ≈3-fold increased ROS production by *NEAT1*$^{-/-}$ compared with WT splenocytes kept under baseline (unstimulated) conditions *in vitro* (*Figure 3F*). Neither PMA nor PMA+LPS stimulation significantly increased ROS production by either strain compared with their respective baseline levels.

Transcriptome mapping of *NEAT1*$^{-/-}$ splenocytes vs. WT identified gross alterations of baseline expression (Supplementary material online, *Table S4A*), and response to LPS stimulation (Supplementary material online, *Table S4B*), for genes encoding CC and CXC chemokines and chemokine receptors (*Figure 3G*), interleukins and their receptors, proteins of early innate immunity and the IFN system, TNF and caspases, and matrix metalloproteinases (Supplementary material online, *Tables S4A* and *B*). In *NEAT1*$^{-/-}$ mice, the chemokines/receptors depicted in *Figure 3G* displayed responses to LPS (down-regulation compared with baseline), which are opposite to their regulation in WT cells. While LPS thus led to down-regulation of multiple chemokines/receptors in *NEAT1*$^{-/-}$ mice, a spectrum of (noncoding) small nucleolar RNAs (SNORDs) became >1000-fold induced in the knockout strain, while remaining unchanged in WT (*Figure 3G*, Supplementary material online, *Table S4B*).

3.4 Studies on *NEAT1*$^{-/-}$ macrophages

3.4.1 Anomalous monocyte-macrophage differentiation in *NEAT1* deficient mice *in vivo*

FACS analysis of blood and bone marrow from *NEAT1*$^{-/-}$ mice, in comparison to WT mice, showed markedly reduced levels of CD45+ monocytes both in the bone marrow ($P = 0.0008$) and in the circulating blood ($P = 0.0093$) of *NEAT1*$^{-/-}$ mice (*Figure 4A–C*). This is reflected by decreased levels of Ly6C^{high} ($P = 0.0060$ in bone marrow; $P = 0.0412$ in blood) and increased levels Ly6C^{low} monocytes in the bone marrow ($P = 0.0056$) and circulating blood ($P = 0.0429$) of *NEAT1*$^{-/-}$ mice. A potential explanation of the observed monocytopenia in *NEAT1*$^{-/-}$ mice is a chronic inflammatory response resulting in increased monocyte mobilization and release from the bone marrow with subsequent systemic trafficking giving rise to tissue macrophages (*Figure 5*).

3.4.2 Disturbed functions of *NEAT1*$^{-/-}$ bone marrow-derived macrophages *ex vivo*

There were multiple functional anomalies in the knockout cells (*Figure 4D–I*). Some of these were present under baseline conditions (*Figure 4D–F*), while others emerged upon LPS stimulation (*Figure 4G–I*). At baseline, *NEAT1*$^{-/-}$ BMDMs displayed significantly (Day 0: $P = 0.0013$; Day 1: $P = 0.02$) lower proliferation rate compared with WT cells (*Figure 4D*), but higher phagocytosis activity ($P < 0.0001$) (*Figure 4F*). The yield of BMDMs derived from a given number of *NEAT1*$^{-/-}$ bone marrow cells was increased ($P = 0.0056$) compared with WT (*Figure 4E*).

NEAT1$^{-/-}$ BMDMs responded to LPS with strongly increased ($P < 0.0001$) ROS production and increased ($P = 0.0016$) NOS2 mRNA expression (*Figure 4G*). While *NEAT1*$^{-/-}$ cells displayed higher baseline phagocytosis activity (*Figure 4F*), their response to LPS was attenuated ($P = 0.0318$) (*Figure 4H*).

RNA-seq detected multiple anomalies in *NEAT1*$^{-/-}$ BMDMs under baseline conditions (*Figure 4I*, Supplementary material online, *Table S5A*) and upon stimulation with LPS (*Figure 4I*, Supplementary material online, *Table S5B*). Partially overlapping with the changes observed in *NEAT1*$^{-/-}$ splenocytes, there was deregulation of several CC and CXC type chemokine/receptor systems in *NEAT1*$^{-/-}$ BMDMs at baseline. Upon LPS stimulation, deregulation of these systems persisted (Supplementary material online, *Table S5B*).

3.5 Histological and immunohistological studies in *NEAT1*$^{-/-}$ mice

NEAT1$^{-/-}$ mice displayed anomalous CD68+ monocyte-macrophage infiltration in the aortic wall (*Figure 5A* and *B* and Supplementary material online, *Figure S2*), in the absence of other evidence of vascular pathology, e.g. atherosclerosis in these animals. Vascular CD68+ cell infiltration was regularly observed (*Figure 5A* and *B*). In addition, there was evidence of major myocardial structural damage in some of the *NEAT1*$^{-/-}$ mice (*Figure 5D*), with substitution of normal myocardial tissue by brown adipose tissue as documented by ADRP staining (*Figure 5E*) and siderophage infiltration in the border zone of the injured area (*Figure 5F*) (for further histological and immunohistological stainings, see Supplementary material online, *Figure S3A–E*).

3.6 Small *NEAT1*-derived menRNA influences the cellular innate immune response

The *NEAT1* gene locus has complex structure and regulation (Supplementary material online, *Figures S4* and *S5*), with two different long primary RNA transcripts and a short enzymatic processing product with a tRNA-like structure designated '*menRNA*' (Supplementary material online, *Figure S5B*). All results above refer to a situation where this entire locus and all its products are deleted. In addition, we investigated

cells in which only this *NEAT1* product menRNA was overexpressed (Supplementary material online, *Figures S6* and *S7*), or deleted by antisense technology (Supplementary material online, *Figure S8*). While the results are preliminary, they show that not only complete deletion of *NEAT1* disturbs immune cell functions, but menRNA deletion alone (Supplementary material online, *Figure S8*) suffices to alter immune gene expression.

4. Discussion

4.1 Anomalous circulating immune cell transcriptomes in early onset MI patients

In an effort to understand the possible role of lncRNAs in the context of atherosclerosis and MI, a first prescreening of test cohorts showed suppression of *NEAT1* in PBMCs of post-MI patients. Subsequent RNA-seq confirmed this and identified seven other lncRNAs significantly deregulated post-MI. Among these *NEAT1* had the highest expression level and was strongly enriched in monocytes. In a third step, *NEAT1* suppression was confirmed in independent validation cohorts. Multivariate statistical analysis revealed that its abundance in PBMCs was significantly ($P = 0.001$) influenced by post-MI status independent of statin intake, LVEF, LDL or HDL cholesterol, smoking, diabetes, or age (*Table 1*). This is consistent with the hypothesis that the observed *NEAT1* suppression reflects or contributes to an immunological disturbance which persists post-MI despite standard post-MI medical therapy.

A clinically relevant aspect of our study design is the selection of patients with early onset MI. These post-MI patients were identified through population-wide screening projects (*MI Young, GIS*) and are about two decades younger than in previous somewhat similar work.[28,29] From the clinical perspective it will be interesting to examine, whether a PBMC expression profile encompassing the most distinctive genes reported here might have prognostic value regarding the clinical course or response to anti-inflammatory treatment. Beyond the IL1β system which is of particular current interest,[9–13,30] other chemokines and interleukins deserve attention. Of note, CXCL2 and IL8[31,32] are robustly expressed in patient but almost undetectable in control PBMCs. PBMCs may thus be a source of CXCL2 and IL8 which increased in sera of patients with cerebro-cardiovascular events.[14] Circulating IL8 is also increased in diabetic patients and associated with worse inflammatory and cardiometabolic profile.[33] Regarding IL8 it is unfortunate that due to incomplete genome homology between mice and men,[34] this particularly strongly deregulated human cytokine has no homologue in mice and the murine *NEAT1* knockout studies below cannot provide direct information on its regulation.

Apart from these translational considerations which of course require testing in a *prospective* trial, the transcriptome maps have already identified one lncRNA *NEAT1* with so far largely unknown biological functions and possible pathogenic relevance in atherosclerosis and MI. The clinical part of this study thus provided a translationally relevant rationale for more in-depth investigations of *NEAT1* functions *in vivo*, by use of our genetic animal knockout model and associated cell culture work.

An important methodological aspect is the fact that RNA-seq allows acquisition of truly comprehensive transcriptome. This overcomes technical limitations of former microarray-based work[28,29] which has not covered the entire transcriptome and was critically limited regarding quantification, due to the far lower dynamic range of detection of microarrays when compared with RNA-seq. This is particularly relevant considering the very broad range of lncRNA expression levels identified in our study (*Figure 1D*). Another RNA-seq based study has addressed myocardial transcriptomes post-MI and identified novel heart-specific lncRNAs,[4] but in that work no data on circulating immune cells were provided.

Here, we provide combined human and mechanistic studies on a systems-level focusing on immune regulation. This is particularly of interest given the emerging clinical concept of residual inflammatory risk in high-risk patients with cardiovascular disease,[9] based on elevated systemic inflammation beyond cholesterol-driven vascular inflammation in atherosclerosis. Marked deregulation of multiple immune-related transcripts in our post-MI patient PBMCs further supports the 'residual inflammatory risk' concept beyond the already well-studied IL1ß (a major cytokine contributing to residual inflammatory risk). *NEAT1* appears as component of a molecular circuit also involving important chemokines (CXCL2, CCR6, CXCR2)[35–37] and interleukins (IL1B, IL8, IL4R, IL7R) remaining disturbed post-MI (further references in the Supplementary material online). Individual profiling of this circuit may contribute, beyond current serum-based markers, to identify high-risk patients likely to benefit from immunomodulatory therapies (*Figures 6* and *7*).

4.2 Immune system dysfunction in a genetic animal model of *NEAT1* deficiency

Prompted by the statistically highly significant association of reduced *NEAT1* expression with early onset MI, we took first steps to study potential mechanistic impact of *NEAT1* depletion in patient PBMCs by investigation of *NEAT1*$^{-/-}$ mice. We employed the *NEAT1*$^{-/-}$ model by Nakagawa *et al.*[5,6] to evaluate whether isolated genetic *NEAT1* deficiency *per se* might causally alter any functions of the immune system. The choice of *NEAT1* was obvious as the most highly expressed deregulated lncRNA in PBMCs, for which an animal model and information regarding its post-transcriptional processing are available.[5,25–27] For the other lncRNAs deregulated in patient PBMCs there is currently no animal model or functional information, and no information regarding transcriptional regulation and processing.[5,38,39]

Most previous research on *NEAT1* focused on mechanistic studies in cell culture models,[3,40–43] whereas insight into the biological functions and possible pathogenic relevance of *NEAT1* are sparse.[44–47] In that regard, our study provides the first data from cardiovascular patients documenting anomalous regulation of *NEAT1* in their PBMCs despite standard post-MI medical therapy, and first evidence of immune system dysfunction in *NEAT1* deficient animals *in vivo*.

Cumulatively, our experimental findings suggest that *NEAT1* is critically involved in regulatory processes of splenocytic cytokine/chemokine (e.g. IFNγ) expression subsequently resulting in altered differentiation and expansion of $CD4^+$ cells of the adaptive immune system. Furthermore, the level of bone marrow and blood monocytes is indicative of potentially altered monocyte efflux, migration and trafficking in *NEAT1*$^{-/-}$ animals. Marked deregulation of multiple chemokines/chemokine receptors on *NEAT1*$^{-/-}$ splenocytes and macrophages, and CD68+ macrophage infiltration of the aortic wall, lends further support to the concept of anomalous immune cell trafficking (*Figure 7*). Irrespective of their *in vivo* migration pattern, however, several functions of *NEAT1*$^{-/-}$ splenocytes and macrophages *per se* are disturbed, e.g. ROS production and NOS2 expression. Furthermore, the increased circulating IFNγ level of *NEAT1*$^{-/-}$ mice indicates impaired inflammation control (*Figure 6* and *7*)

even though these animals were kept *without* external immunological stress, e.g. high cholesterol diet, viral infection, or ischaemia. The fragility and survival disadvantage of the *NEAT1*$^{-/-}$ strain is emphasized by the fact that crossbreeding into ApoE$^{-/-}$ mice remained unsuccessful despite major efforts, and that the reproductive capacity of *NEAT1*$^{-/-}$ animals is significantly reduced compared with WT. As *homozygous NEAT1* deletion obviously renders the organism highly vulnerable, it appears reasonable to investigate the effects of *heterozygous NEAT1* deficiency upon murine disease models instead.

4.3 Consequences of *NEAT1* deficiency at the cellular and molecular level

At the molecular level, mechanistic insight into immunological functions of *NEAT1* is particularly difficult to obtain because the *NEAT1* locus does not only generate two long noncoding transcripts with important nucleolar structural functions[48–50] and cell type-specific expression, but furthermore generates a small tRNA-like processing product located in the cytosol (*Figure 6*, Supplementary material online, *Figures S5* and *S6*). Thus, complete germline *NEAT1* deletion will necessarily severely affect multiple components of this complex integrated RNA transcription and processing system. Major impact of *NEAT1* deficiency on nucleolar function is suggested by massive >1000-fold induction by LPS of a broad spectrum of small nucleolar RNAs (snoRNAs)[51,52] in the knockout strain, while they remained unchanged in WT (*Figure 3G*, Supplementary material online, *Table S4B*). C/D box snoRNAs (SNORDs) are an abundantly expressed class of RNAs that can regulate pre-mRNA alternative splicing, mRNA abundance, activate enzymes, and be processed into short ncRNAs resembling miRNAs and piRNAs.[51] A recent study on genetic associations suggested an independent role for 14q32 snoRNAs in human cardiovascular diseases.[52] The *NEAT1* system is evolutionary highly conserved, suggesting important functions in complex organisms. When the extensive transcriptome alterations of *NEAT1*$^{-/-}$ splenocytes and macrophages are considered in the context of their functional disturbances at the cellular level, it appears reasonable to assume that *NEAT1* is required for optimal coordination of multiple immune system functions at the RNA level. Systems biology approaches towards our RNA-seq datasets would not appear promising due to the currently still profound lack of sufficient experimental data regarding lncRNAs interactions with other RNAs (including mRNAs)[48–50] as well as proteins.[53]

At the cellular level, however, we have already obtained evidence of anomalous T cell differentiation and expansion in *NEAT1* deficient mice *in vivo* and altered ROS production by splenocytes, in association with extensive re-programming of the splenocyte transcriptome in *NEAT1*$^{-/-}$ mice. Splenocytes also displayed markedly increased IFNγ expression consistent with increased circulating IFNγ in this strain.

Regarding the monocyte-macrophage lineage, *NEAT1*$^{-/-}$ mice display anomalous monocyte-macrophage differentiation in bone marrow and blood. A possible explanation of the monocytopenia in *NEAT1*$^{-/-}$ mice is a chronic inflammatory response (consistent with high circulating IFNγ) leading to increased monocyte mobilization and release from the bone marrow and subsequent systemic trafficking giving rise to tissue macrophages, e.g. CD68+ cells in the vascular wall. Functional analyses of BMDMs from *NEAT1*$^{-/-}$ mice further detected a massive increase of macrophage ROS production in response to LPS. This is proof that *NEAT1* deficiency causes impaired control of a key function of macrophages, i.e. the generation of ROS in response to an inflammatory stimulus. In line with this, inducible NOS (iNOS) expression was up-regulated in LPS-stimulated *NEAT1*$^{-/-}$ BMDMs compared with WT cells. Reduced levels of *NEAT1* in the post-MI patient PBMCs may have the potential to cause de-repression of ROS production, which in turn may lead to more aggressive action of circulating monocytes-macrophages against their targets, e.g. within the vascular wall. Of note, ROS not only plays a critical role in the differentiation of alternatively activated macrophages, but also in the occurrence of tumour-associated macrophages.[54–56] Thus, *NEAT1* deficiency may impact upon the course of diseases (e.g. atherosclerosis, cancer) in which macrophages are pathogenetically involved. Conclusively, our findings provide evidence that *NEAT1* has major impact on inflammatory processes that encompass components of both the innate and acquired immune systems.

4.4 Working model and translational aspects

The results of our studies in humans and mice are briefly summarized in *Figure 6*. The animal model and cell culture data support a working model (*Figure 7*) which encompasses disturbances in bone marrow, spleen, and blood circulation of the *NEAT1* deficient mice. In the spleen, there is anomalous T cell differentiation leading to increased circulation of Th cells. Splenocytic IFNγ expression and ROS production is increased already under baseline conditions. There is anomalous monocyte-macrophage differentiation in the bone marrow, and *NEAT1*$^{-/-}$ macrophages display enhanced ROS production and NOS2 expression. Once the *NEAT1*-deficient cells enter the circulation, their altered chemokine and chemokine receptor expression pattern should significantly affect their trafficking and may explain the detection of CD68+ macrophages in the vasculature of *NEAT1* deficient mice.

The 'baseline' scenario of *Figure 7* described the situation in animals *not* exposed to external immunological stress. Due to the fragility and survival disadvantage of *NEAT1*$^{-/-}$ mice it will be technically demanding to find out how this 'unstable' anomalous immune system reacts to stress. Preliminary insight from our *NEAT1*$^{-/+}$ ApoE$^{-/-}$ strain suggests that even heterozygous *NEAT1* deficiency leads to systemic inflammation with high IFNγ levels when exposed to high cholesterol challenge (Supplementary material online, *Figure S3A*). The observation of occasional grave myocardial structural injury suggests that even stochastic activation of the highly unstable *NEAT1*$^{-/-}$ immune system may trigger an uncontrolled pathogenic cascade. This may also well explain the notorious difficulties encountered in the breeding and cross-breeding of *NEAT1*-deficient mice. Our present focus on cardiovascular disturbances may have failed to adequately appreciate the fact of systemic inflammation with elevated IFNγ levels in *NEAT1*$^{-/-}$ mice which strongly suggests systematic histopathological investigation of multiple organs in these animals. In particular, this should be conducted at different ages and under immunological challenges, e.g. high-fat diet. Future work has to clarify which other disease models may be tolerated by the fragile *NEAT1* strain, and which further insight they may provide regarding the *NEAT1* system. Independent of additional results from future experimental work, *NEAT1* is obviously a significant novel component of a PBMC-based immunoregulatory network which remains markedly 'out-of-balance' after MI despite standard therapy.

In conclusion, this first comprehensive transcriptome study of circulating immune cells from early onset MI patients indicates distinctive alterations of lncRNA expression in their PBMCs. The experimental data from *NEAT1*$^{-/-}$ mice provide first direct evidence that *NEAT1* is a novel lncRNA-type immunoregulator affecting T cell and monocyte-macrophage lineage differentiation and functions *in vivo*. Consistent with this, *NEAT1* suppression in post-MI patients may reflect an 'out-of-

balance' status of their immune system, persisting post-MI despite standard therapy. It appears warranted to further investigate whether dysregulation of the *NEAT1* system has pathogenic potential and thus might constitute a novel therapeutic target.

Supplementary material

Supplementary material is available at *Cardiovascular Research* online.

Authors' contributions

W.P. and T.Z. and designed the research and drafted the manuscript. M.G., B.R., A.H., S.N., and U.L. made critical revisions to the manuscript. S.N. and T.H. developed the *NEAT1* knockout animal model. T.Z., S.B., C.M., and D.B. conducted and analysed the clinical studies from which the test and validation patient and control cohorts were derived. J.H. and B.M. conducted the RNA-seq of human PBMCs. A.Kuss, L.J., and S.W. conducted the RNA-seq of murine splenocytes and macrophages. A.H., D.S., and P.S. conducted the FACS analyses of murine bone marrow, spleen, and blood. FE, A.Kühl, A.K., and N.K. contributed to the histological and immunohistological studies. A.S., M.G., A.K., and C.M. performed statistical analyses.

Acknowledgements

We thank Ms Xiaomin Wang, Ms Susanne Ochmann, Ms Corinna Jensen, and Mr Georg Zingler for excellent technical assistance.

Conflict of interest: none declared.

Funding

This study was supported by the German Center for Cardiovascular Research (DZHK) through Shared Expertise grant 18-005 to W.P., U.L., T.Z., and S.B. T.Z. is supported by the German Center for Cardiovascular Research (DZHK, 81Z1710101).

References

1. Poller W, Dimmeler S, Heymans S, Zeller T, Haas J, Karakas M, Leistner DM, Jakob P, Nakagawa S, Blankenberg S, Engelhardt S, Thum T, Weber C, Meder B, Hajjar R, Landmesser U. Non-coding RNAs in cardiovascular diseases: diagnostic and therapeutic perspectives. *Eur Heart J* 2018;**39**:2704–2716.
2. Gast M, Schroen B, Voigt A, Haas J, Kuehl U, Lassner D, Skurk C, Escher F, Wang X, Kratzer A, Michalik K, Papageorgiou A, Peters T, Loebel M, Wilk S, Althof N, Prasanth KV, Katus H, Meder B, Nakagawa S, Scheibenbogen C, Schultheiss HP, Landmesser U, Dimmeler S, Heymans S, Poller W. Long noncoding RNA MALAT1-derived mascRNA is involved in cardiovascular innate immunity. *J Mol Cell Biol* 2016;**8**:178–181.
3. Imamura K, Imamachi N, Akizuki G, Kumakura M, Kawaguchi A, Nagata K, Kato A, Kawaguchi Y, Sato H, Yoneda M, Kai C, Yada T, Suzuki Y, Yamada T, Ozawa T, Kaneki K, Inoue T, Kobayashi M, Kodama T, Wada Y, Sekimizu K, Akimitsu N. Long noncoding RNA NEAT1-dependent SFPQ relocation from promoter region to paraspeckle mediates IL8 expression upon immune stimuli. *Mol Cell* 2014;**53**:393–406.
4. Ounzain S, Micheletti R, Beckmann T, Schroen B, Alexanian M, Pezzuto I, Crippa S, Nemir M, Sarre A, Johnson R, Dauvillier J, Burdet F, Ibberson M, Guigo R, Xenarios I, Heymans S, Pedrazzini T. Genome-wide profiling of the cardiac transcriptome after myocardial infarction identifies novel heart-specific long non-coding RNAs. *Eur Heart J* 2015;**36**:353–368a.
5. Nakagawa S, Shimada M, Yanaka K, Mito M, Arai T, Takahashi E, Fujita Y, Fujimori T, Standaert L, Marine JC, Hirose T. The lncRNA Neat1 is required for corpus luteum formation and the establishment of pregnancy in a subpopulation of mice. *Development* 2014;**141**:4618–4627.
6. Nakagawa S. Lessons from reverse-genetic studies of lncRNAs. *Biochim Biophys Acta* 2016;**1859**:177–183.
7. Bobbert P, Scheibenbogen C, Jenke A, Kania G, Wilk S, Krohn S, Stehr J, Kuehl U, Rauch U, Eriksson U, Schultheiss HP, Poller W, Skurk C. Adiponectin expression in patients with inflammatory cardiomyopathy indicates favourable outcome and inflammation control. *Eur Heart J* 2011;**32**:1134–1147.
8. Heimesaat MM, Grundmann U, Alutis ME, Fischer A, Bereswill S. Small intestinal pro-inflammatory immune responses following campylobacter jejuni infection of secondary abiotic IL-10(-/-) mice lacking nucleotide-oligomerization-domain-2. *Eur J Microbiol Immunol (Bp)* 2017;**7**:138–145.
9. Ridker PM, Everett BM, Thuren T, MacFadyen JG, Chang WH, Ballantyne C, Fonseca F, Nicolau J, Koenig W, Anker SD, Kastelein JJP, Cornel JH, Pais P, Pella D, Genest J, Cifkova R, Lorenzatti A, Forster T, Kobalava Z, Vida-Simiti L, Flather M, Shimokawa H, Ogawa H, Dellborg M, Rossi PRF, Troquay RPT, Libby P, Glynn RJ, Group CT. Antiinflammatory therapy with canakinumab for atherosclerotic disease. *N Engl J Med* 2017;**377**:1119–1131.
10. Ridker PM, Libby P, MacFadyen JG, Thuren T, Ballantyne C, Fonseca F, Koenig W, Shimokawa H, Everett BM, Glynn RJ. Modulation of the interleukin-6 signalling pathway and incidence rates of atherosclerotic events and all-cause mortality: analyses from the Canakinumab Anti-Inflammatory Thrombosis Outcomes Study (CANTOS). *Eur Heart J* 2018;**39**:3499–3507.
11. Everett BM, Donath MY, Pradhan AD, Thuren T, Pais P, Nicolau JC, Glynn RJ, Libby P, Ridker PM. Anti-inflammatory therapy with canakinumab for the prevention and management of diabetes. *J Am Coll Cardiol* 2018;**71**:2392–2401.
12. Ridker PM, MacFadyen JG, Glynn RJ, Koenig W, Libby P, Everett BM, Lefkowitz M, Thuren T, Cornel JH. Inhibition of interleukin-1beta by canakinumab and cardiovascular outcomes in patients with chronic kidney disease. *J Am Coll Cardiol* 2018;**71**:2405–2414.
13. Gomez D, Baylis RA, Durgin BG, Newman AAC, Alencar GF, Mahan S, St Hilaire C, Muller W, Waisman A, Francis SE, Pinteaux E, Randolph GJ, Gram H, Owens GK. Interleukin-1beta has atheroprotective effects in advanced atherosclerotic lesions of mice. *Nat Med* 2018;**24**:1418–1429.
14. Szomjak E, Der H, Kerekes G, Veres K, Csiba L, Toth J, Peter M, Soltesz P, Szodoray P. Immunological parameters, including CXCL8 (IL-8) characterize cerebro- and cardiovascular events in patients with peripheral artery diseases. *Scand J Immunol* 2010;**71**:283–291.
15. Broughton SE, Hercus TR, Hardy MP, McClure BJ, Nero TL, Dottore M, Huynh H, Braley H, Barry EF, Kan WL, Dhagat U, Scotney P, Hartman D, Busfield SJ, Owczarek CM, Nash AD, Wilson NJ, Parker MW, Lopez AF. Dual mechanism of interleukin-3 receptor blockade by an anti-cancer antibody. *Cell Rep* 2014;**8**:410–419.
16. Moreno-Viedma V, Amor M, Sarabi A, Bilban M, Staffler G, Zeyda M, Stulnig TM. Common dysregulated pathways in obese adipose tissue and atherosclerosis. *Cardiovasc Diabetol* 2016;**15**:120.
17. Li J, Ley K. Lymphocyte migration into atherosclerotic plaque. *Arterioscler Thromb Vasc Biol* 2015;**35**:40–49.
18. Lacy M, Kontos C, Brandhofer M, Hille K, Groning S, Sinitski D, Bourilhon P, Rosenberg E, Krammer C, Thavayogarajah T, Pantouris G, Bakou M, Weber C, Lolis E, Bernhagen J, Kapurniotu A. Identification of an Arg-Leu-Arg tripeptide that contributes to the binding interface between the cytokine MIF and the chemokine receptor CXCR4. *Sci Rep* 2018;**8**:5171.
19. Regan-Komito D, Valaris S, Kapellos TS, Recio C, Taylor L, Greaves DR, Iqbal AJ. Absence of the non-signalling chemerin receptor CCRL2 exacerbates acute inflammatory responses *in vivo*. *Front Immunol* 2017;**8**:1621.
20. Girbl T, Lenn T, Perez L, Rolas L, Barkaway A, Thiriot A, Del Fresno C, Lynam E, Hub E, Thelen M, Graham G, Alon R, Sancho D, von Andrian UH, Voisin MB, Rot A, Nourshargh S. Distinct compartmentalization of the chemokines CXCL1 and CXCL2 and the atypical receptor ACKR1 determine discrete stages of neutrophil diapedesis. *Immunity* 2018;**49**:1062–1076.e6.
21. Schreiber G. The molecular basis for differential type I interferon signaling. *J Biol Chem* 2017;**292**:7285–7294.
22. Lai Y, Xue C, Liao Y, Huang L, Peng Q, Huang B, Wei S, He L, Gong A, Wang M. Differential expression of Toll-like receptor signaling pathway is associated with microscopic polyangiitis in peripheral blood neutrophils. *Immunol Invest* 2017;**46**:375–384.
23. Chistiakov DA, Myasoedova VA, Revin VV, Orekhov AN, Bobryshev YV. The impact of interferon-regulatory factors to macrophage differentiation and polarization into M1 and M2. *Immunobiology* 2018;**223**:101–111.
24. Azghandi S, Prell C, van der Laan SW, Schneider M, Malik R, Berer K, Gerdes N, Pasterkamp G, Weber C, Haffner C, Dichgans M. Deficiency of the stroke relevant HDAC9 gene attenuates atherosclerosis in accord with allele-specific effects at 7p21.1. *Stroke* 2015;**46**:197–202.
25. Wilusz JE. Long noncoding RNAs: re-writing dogmas of RNA processing and stability. *Biochim Biophys Acta* 2016;**1859**:128–138.
26. Kuhn CD, Wilusz JE, Zheng Y, Beal PA, Joshua-Tor L. On-enzyme refolding permits small RNA and tRNA surveillance by the CCA-adding enzyme. *Cell* 2015;**160**:644–658.
27. Wilusz JE, Whipple JM, Phizicky EM, Sharp PA. tRNAs marked with CCACCA are targeted for degradation. *Science* 2011;**334**:817–821.

28. Cai Y, Yang Y, Chen X, Wu G, Zhang X, Liu Y, Yu J, Wang X, Fu J, Li C, Jose PA, Zeng C, Zhou L. Circulating 'lncRNA OTTHUMT00000387022' from monocytes as a novel biomarker for coronary artery disease. *Cardiovasc Res* 2016;**112**:714–724.
29. Yang Y, Cai Y, Wu G, Chen X, Liu Y, Wang X, Yu J, Li C, Chen X, Jose PA, Zhou L, Zeng C. Plasma long non-coding RNA, CoroMarker, a novel biomarker for diagnosis of coronary artery disease. *Clin Sci* 2015;**129**:675–685.
30. Schofer N, Ludwig S, Rubsamen N, Schnabel R, Lackner KJ, Ruprecht HJ, Bickel C, Landmesser U, Blankenberg S, Zeller T. Prognostic impact of interleukin-1 receptor antagonist in patients with documented coronary artery disease. *Int J Cardiol* 2018; **257**:24–29.
31. Wang L, Zhang YL, Lin QY, Liu Y, Guan XM, Ma XL, Cao HJ, Liu Y, Bai J, Xia YL, Du J, Li HH. CXCL1-CXCR2 axis mediates angiotensin II-induced cardiac hypertrophy and remodelling through regulation of monocyte infiltration. *Eur Heart J* 2018;**39**: 1818–1831.
32. Fu S, Lin J. Blocking interleukin-6 and interleukin-8 signaling inhibits cell viability, colony-forming activity, and cell migration in human triple-negative breast cancer and pancreatic cancer cells. *Anticancer Res* 2018;**38**:6271–6279.
33. Cimini FA, Barchetta I, Porzia A, Mainiero F, Costantino C, Bertoccini L, Ceccarelli V, Morini S, Baroni MG, Lenzi A, Cavallo MG. Circulating IL-8 levels are increased in patients with type 2 diabetes and associated with worse inflammatory and cardiometabolic profile. *Acta Diabetol* 2017;**54**:961–967.
34. Ernst PB, Carvunis AR. Of mice, men and immunity: a case for evolutionary systems biology. *Nat Immunol* 2018;**19**:421–425.
35. Sjaarda J, Gerstein H, Chong M, Yusuf S, Meyre D, Anand SS, Hess S, Pare G. Blood CSF1 and CXCL12 as causal mediators of coronary artery disease. *J Am Coll Cardiol* 2018;**72**:300–310.
36. Zhang M, Nakamura K, Kageyama S, Lawal AO, Gong KW, Bhetraratana M, Fujii T, Sulaiman D, Hirao H, Bolisetty S, Kupiec-Weglinski JW, Araujo JA. Myeloid HO-1 modulates macrophage polarization and protects against ischemia-reperfusion injury. *JCI Insight* 2018;**3**. doi:10.1172/jci.insight.120596.
37. Liu Y, Carmona-Rivera C, Moore E, Seto NL, Knight JS, Pryor M, Yang ZH, Hemmers S, Remaley AT, Mowen KA, Kaplan MJ. Myeloid-specific deletion of peptidylarginine deiminase 4 mitigates atherosclerosis. *Front Immunol* 2018;**9**:1680.
38. Nakagawa S, Ip JY, Shioi G, Tripathi V, Zong X, Hirose T, Prasanth KV. Malat1 is not an essential component of nuclear speckles in mice. *RNA* 2012;**18**:1487–1499.
39. Zong X, Nakagawa S, Freier SM, Fei J, Ha T, Prasanth SG, Prasanth KV. Natural antisense RNA promotes 3' end processing and maturation of MALAT1 lncRNA. *Nucleic Acids Res* 2016;**44**:2898–2908.
40. Wang L, Xia JW, Ke ZP, Zhang BH. Blockade of NEAT1 represses inflammation response and lipid uptake via modulating miR-342-3p in human macrophages THP-1 cells. *J Cell Physiol* 2019;**234**:5319–5326.
41. Zhou ZW, Zheng LJ, Ren X, Li AP, Zhou WS. LncRNA NEAT1 facilitates survival and angiogenesis in oxygen-glucose deprivation (OGD)-induced brain microvascular endothelial cells (BMECs) via targeting miR-377 and upregulating SIRT1, VEGFA, and BCL-XL. *Brain Res* 2019;**1707**:90–98.
42. Yong W, Yu D, Jun Z, Yachen D, Weiwei W, Midie X, Xingzhu J, Xiaohua W. Long non-coding RNA NEAT1, regulated by LIN28B, promotes cell proliferation and migration through sponging miR-506 in high-grade serous ovarian cancer. *Cell Death Dis* 2018;**9**:861.
43. Yan W, Chen ZY, Chen JQ, Chen HM. LncRNA NEAT1 promotes autophagy in MPTP-induced Parkinson's disease through stabilizing PINK1 protein. *Biochem Biophys Res Commun* 2018;**496**:1019–1024.
44. Adriaens C, Standaert L, Barra J, Latil M, Verfaillie A, Kalev P, Boeckx B, Wijnhoven PW, Radaelli E, Vermi W, Leucci E, Lapouge G, Beck B, van den Oord J, Nakagawa S, Hirose T, Sablina AA, Lambrechts D, Aerts S, Blanpain C, Marine JC. p53 induces formation of NEAT1 lncRNA-containing paraspeckles that modulate replication stress response and chemosensitivity. *Nat Med* 2016;**22**:861–868.
45. Yu X, Li Z, Zheng H, Chan MT, Wu WK. NEAT1: a novel cancer-related long non-coding RNA. *Cell Prolif* 2017;**50**. doi:10.1111/cpr.12329.
46. Sunwoo JS, Lee ST, Im W, Lee M, Byun JI, Jung KH, Park KI, Jung KY, Lee SK, Chu K, Kim M. Altered expression of the long noncoding RNA NEAT1 in Huntington's disease. *Mol Neurobiol* 2017;**54**:1577–1586.
47. Chakravarty D, Sboner A, Nair SS, Giannopoulou E, Li R, Hennig S, Mosquera JM, Pauwels J, Park K, Kossai M, MacDonald TY, Fontugne J, Erho N, Vergara IA, Ghadessi M, Davicioni E, Jenkins RB, Palanisamy N, Chen Z, Nakagawa S, Hirose T, Bander NH, Beltran H, Fox AH, Elemento O, Rubin MA. The oestrogen receptor alpha-regulated lncRNA NEAT1 is a critical modulator of prostate cancer. *Nat Commun* 2014;**5**:5383.
48. Yamazaki T, Souquere S, Chujo T, Kobelke S, Chong YS, Fox AH, Bond CS, Nakagawa S, Pierron G, Hirose T. Functional domains of NEAT1 architectural lncRNA induce paraspeckle assembly through phase separation. *Mol Cell* 2018;**70**: 1038–1053.e7.
49. Yamazaki T, Fujikawa C, Kubota A, Takahashi A, Hirose T. CRISPRa-mediated NEAT1 lncRNA upregulation induces formation of intact paraspeckles. *Biochem Biophys Res Commun* 2018;**504**:218–224.
50. Nakagawa S, Yamazaki T, Hirose T. Molecular dissection of nuclear paraspeckles: towards understanding the emerging world of the RNP milieu. *Open Biol* 2018;**8**. doi:10.1098/rsob.180150.
51. Falaleeva M, Welden JR, Duncan MJ, Stamm S. C/D-box snoRNAs form methylating and non-methylating ribonucleoprotein complexes: old dogs show new tricks. *Bioessays* 2017;**39**. doi:10.1002/bies.201600264.
52. Hakansson KEJ, Goossens EAC, Trompet S, van Ingen E, de Vries MR, van der Kwast R, Ripa RS, Kastrup J, Hohensinner PJ, Kaun C, Wojta J, Bohringer S, Le Cessie S, Jukema JW, Quax PHA, Nossent AY. Genetic associations and regulation of expression indicate an independent role for 14q32 snoRNAs in Human Cardiovascular Disease. *Cardiovasc Res* 2019;**115**:1519–1532.
53. Spiniello M, Knoener RA, Steinbrink MI, Yang B, Cesnik AJ, Buxton KE, Scalf M, Jarrard DF, Smith LM. HyPR-MS for multiplexed discovery of MALAT1, NEAT1, and NORAD lncRNA protein interactomes. *J Proteome Res* 2018;**17**:3022–3038.
54. Covarrubias A, Byles V, Horng T. ROS sets the stage for macrophage differentiation. *Cell Res* 2013;**23**:984–985.
55. Zhang Y, Choksi S, Chen K, Pobezinskaya Y, Linnoila I, Liu ZG. ROS play a critical role in the differentiation of alternatively activated macrophages and the occurrence of tumor-associated macrophages. *Cell Res* 2013;**23**:898–914.
56. Tschopp J, Schroder K. NLRP3 inflammasome activation: the convergence of multiple signalling pathways on ROS production? *Nat Rev Immunol* 2010;**10**: 210–215.

Corrigendum

doi:10.1093/cvr/cvz189
Online publish-ahead-of-print 29 July 2019

Corrigendum to: Low cardiac lipolysis reduces mitochondrial fission and prevents lipotoxic heart dysfunction in Perilipin 5 mutant mice [*Cardiovasc Res* 2019;doi:10.1093/cvr/cvz119]

In the original version of the above article, Matthias Schittmayer was inadvertently omitted from the author list. This has now been corrected online and in print.

The authors apologise for the error.